crystals

MDPI

Review

A Comprehensive Review of Sulfide Solid-State Electrolytes: Properties, Synthesis, Applications, and Challenges

Bin Man [1], Yulong Zeng [1], Qingrui Liu [1], Yinwen Chen [1], Xin Li [1], Wenjing Luo [1], Zikang Zhang [1], Changliang He [1], Min Jie [2] and Sijie Liu [2,3,*]

[1] School of Aerospace Engineering & High-Performance Battery Laboratory, Geely University, Chengdu 641423, China; manbin@guc.edu.cn (B.M.); zengyulong@guc.freeqiye.com (Y.Z.); liuqingrui@guc1.freeqiye.com (Q.L.); chenyinwen@guc666.freeqiye.com (Y.C.); lixin@guc02.freeqiye.com (X.L.); luowenjing@guc01.freeqiye.com (W.L.); zhangzikan@guc3.freeqiye.com (Z.Z.); hechangliang@guc.edu.cn (C.H.)
[2] Research Institute of Tsinghua University in Shenzhen, Shenzhen 518000, China; nichomj@163.com
[3] Institute of Nuclear and New Energy Technology, Tsinghua University, Beijing 100084, China
* Correspondence: liusijie@mail.tsinghua.edu.cn

Abstract: Traditional lithium-ion batteries (LIBs) utilize liquid electrolytes, which pose significant safety risks. To address these concerns and enhance energy density, all-solid-state batteries (ASSBs) have emerged as a safer and more efficient alternative to conventional liquid electrolyte-based systems. ASSBs offer notable advantages, including higher energy density and improved safety, driving growing interest from both industry and academia. A key component in all-solid-state battery (ASSB) development is the solid-state electrolyte (SSE), which plays a crucial role in determining the overall performance and safety of these batteries. Sulfide SSEs are characterized by distinctive attributes, including notably high ionic conductivity and remarkably low interfacial resistance with lithium metal anodes, which renders them particularly advantageous for advancing ASSB technology. This paper systematically examines sulfide-based SSEs, with particular emphasis on their underlying physicochemical properties, structural characteristics, and essential functional attributes relevant to ASSB applications. Additionally, we explore preparation methods for sulfide SSEs and analyze their potential applications in next-generation ASSBs. Considering current challenges (e.g., interfacial instability or air sensitivity) we summarize strategies to address these obstacles, aiming to facilitate their integration into future energy storage systems.

Keywords: ASSB; sulfide SSE; ionic conduction mechanism

check for updates

Academic Editor: Dmitri Donetski

Received: 1 April 2025
Revised: 22 April 2025
Accepted: 24 April 2025
Published: 22 May 2025

Citation: Man, B.; Zeng, Y.; Liu, Q.; Chen, Y.; Li, X.; Luo, W.; Zhang, Z.; He, C.; Jie, M.; Liu, S. A Comprehensive Review of Sulfide Solid-State Electrolytes: Properties, Synthesis, Applications, and Challenges. *Crystals* **2025**, *15*, 492. https://doi.org/10.3390/cryst15060492

Copyright: © 2025 by the authors. Licensee MDPI, Basel, Switzerland. This article is an open access article distributed under the terms and conditions of the Creative Commons Attribution (CC BY) license (https://creativecommons.org/licenses/by/4.0/).

1. Introduction

With the rapid advancement of secure, flexible, and scalable electronic devices, the development of efficient energy storage systems to support these innovations has become paramount [1,2]. Among various energy storage solutions, lithium-ion batteries (LIBs) have emerged as a leading technology due to their high energy density and long cycle life. However, traditional LIBs employing liquid electrolytes pose significant risks associated with volatilization and leakage, leading to safety concerns and necessitating complex packaging measures. In response to these challenges, all-solid-state batteries (ASSBs) have attracted increasing attention over the past few decades [3–7]. Figure 1 illustrates the key advancements in sulfide electrolytes in recent years. A key component of ASSBs is the solid-state electrolyte (SSE), which offers a promising alternative by effectively addressing the inherent issues of liquid electrolytes, such as flammability and instability. SSEs enhance

safety and stability while enabling improvements in the performance and reliability of next-generation energy storage systems.

Currently, ASSBs can be classified based on the type of SSE employed, with the primary categories being polymer-based, oxide-based, sulfide-based, and halide-based ASSBs [8,9]. Among these, sulfide-based ASSBs exhibit considerable promise for commercialization due to their superior ionic conductivity, favorable mechanical properties, thermal stability, and moderate production costs [10–19]. Halide-based SSEs also show potential due to their unique ionic transport mechanisms and compatibility with diverse electrode materials [20,21]. Collectively, these advancements position ASSBs as a highly promising solution for meeting the evolving demands of next-generation energy storage applications. Their ability to improve safety, stability, and performance aligns with the requirements of emerging technologies, solidifying their status as a central focus of research and development in the field [22].

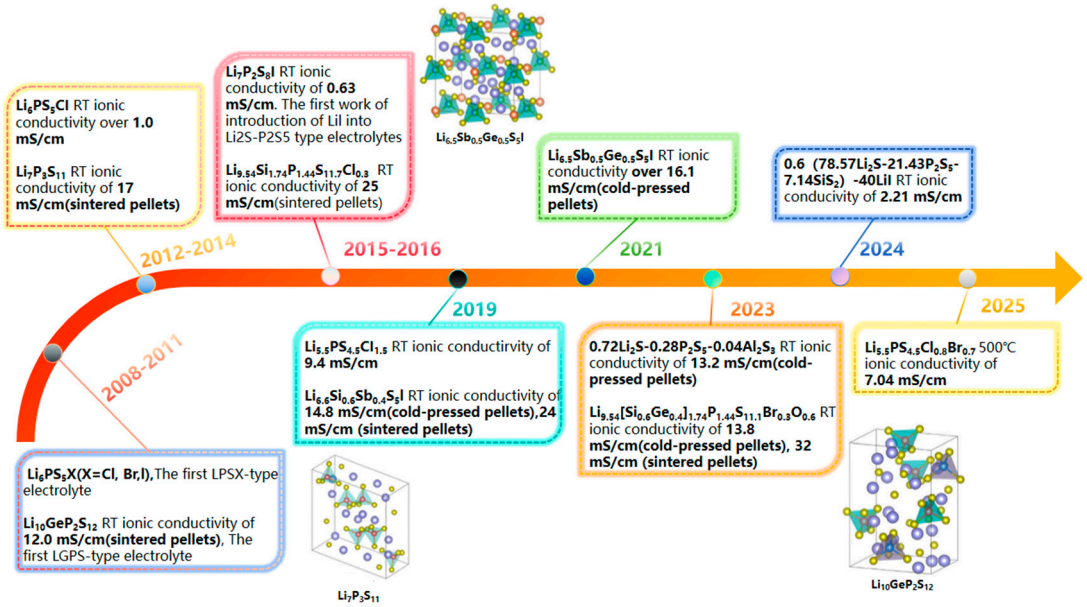


Figure 1. Significant developmental milestones of sulfide electrolytes over the past 20 years [12,23–34].

1.1. Background of SSEs

With the rapid advancement of the global economy, the demand for energy has surged. The accelerated consumption of fossil fuels exacerbates energy supply strain and contributes to environmental pollution and climate change. To achieve sustainable and low-carbon development goals, promoting new energy technologies—such as photovoltaic and wind power—is imperative. These technologies are critical for mitigating environmental degradation and global warming. However, their inherent challenges, including temporal variability and instability in energy output, necessitate complementary solutions. Developing efficient, clean, and renewable energy sources, alongside scalable energy storage technologies, is vital for enhancing national productivity and quality of life while reducing environmental harm.

LIBs, commercialized in the 1990s, dominate the electronics market due to their high operating voltage, large specific energy, long cycle life, and low environmental impact [35]. Innovations in electrolyte materials have been pivotal in advancing LIB performance [36]. Early LIBs relied on liquid organic electrolytes with carbonate solvents, which provided sufficient ionic conductivity for commercialization. Subsequent improvements, particularly through the introduction of functional additives, have focused on increasing energy density, reducing internal resistance, and extending cycle life. Lithium metal anodes, with their high theoretical specific capacity (3860 mAh/g), low potential (−3.04 V vs. standard hydrogen

electrode), and low density (0.53 g/cm^3), are ideal for replacing graphite anodes, potentially doubling battery specific energy from 200 Wh/kg to 400 Wh/kg [37]. Novel solvents (e.g., ethers, nitriles, and sulfones) and advanced electrolyte designs (e.g., high-concentration, localized high-concentration, and weakly solvated electrolytes) have further enhanced electrochemical performance, safety, and stability [38]. Nevertheless, the flammability, leakage, and poor temperature stability of these electrolytes remain unresolved safety concerns [39].

ASSBs, exhibiting superior energy density, enhanced safety profiles, and extended cycle durability, have emerged as leading candidates for next-generation electrochemical energy storage systems [40]. The replacement of liquid electrolytes with SSEs in ASSBs effectively addresses electrolyte leakage and thermal runaway risks while simultaneously mitigating lithium dendrite formation through enhanced interfacial stability [41]. The core of ASSB technology lies in SSE development, including: oxides (e.g., NASICON SSE: $Li_{1.3}Al_{0.3}Ti_{1.7}(PO_4)_3$ [42,43], garnet electrolyte: $Li_7La_3Zr_2O_{12}$ [44]); polymers (e.g., polyethylene oxide (PEO) [45], polyvinylidene fluoride (PVDF) [46]); sulfides (e.g., lithium thiophosphate: $Li_7P_3S_{11}$ [47], $Li_{10}GeP_2S_{12}$(LGPS) [48]); halides (e.g., Li_3InCl_6 [49], Li_3YCl_6 [50], Li_3HoCl_6 [51]).

SSEs must exhibit high ionic conductivity, wide electrochemical windows, robust mechanical properties, and compatibility with electrode materials. Among these characteristics, mechanical robustness and ionic conductivity directly determine the overall battery performance [52].

Polymer SSEs exhibit favorable mechanical properties and effectively suppress lithium dendrite formation [53]. However, their narrow electrochemical window (e.g., the electrochemical window of PEO < 3.9 V) render them susceptible to oxidation when paired with high-voltage cathodes. For instance, severe electrochemical decomposition occurs in systems utilizing cathodes such as $LiCoO_2$ (LCO) [54,55], $LiNi_xCo\gamma Mn_vO_2$ (NCM) [23], or $LiNi_xCo\gamma Al_vO_2$ (NCA) [23], leading to rapid performance degradation [56]. Additionally, polymer SSEs demonstrate inadequate thermal stability: exposure to temperatures exceeding 400 °C triggers decomposition and combustion, posing critical safety risks [57].

Oxide SSEs are favored for their chemical stability, thermal resilience, and versatility, making them a preferred choice for industrial applications. However, high interfacial impedance—stemming from poor electrode–electrolyte wettability due to the rigid and non-fluid nature of oxides—remains a critical barrier to their adoption in ASSBs [58,59]. Approaches to address this issue include interfacial modification layers and densification techniques, such as spark plasma sintering or hot pressing. Furthermore, oxide SSEs require sintering temperatures exceeding 1200 °C, which can induce lithium loss and degrade battery performance [60].

Sulfide SSEs stand out due to their ultrahigh ionic conductivity (>10^{-3} S·cm^{-1}) and machinability, enabling seamless integration into ASSBs [61]. Their advantages include enhanced ionic conductivity—the larger atomic radius and lower electronegativity of sulfur reduce Li^+ binding energy, facilitating ion migration, and superior mechanical properties—ductility and low hardness improve interfacial contact with electrodes [62–64].

Despite their advantages, sulfide-based solid-state electrolytes (SSEs) still face significant challenges, including air sensitivity, interfacial instability (both electrochemical and thermomechanical), and scalability issues, all of which impede their commercial adoption. Overcoming these obstacles necessitates a comprehensive understanding of their structural properties, ion transport mechanisms, and failure modes, coupled with the development of innovative approaches for stabilizing interfaces [65,66].

This review systematically examines the characteristics, synthesis methods, applications, and challenges of sulfide SSEs, and summarizes future directions for sulfide-based ASSBs. Sulfide SSE synthesis is typically employed to prevent moisture-induced degrada-

tion [67]. Liquid-phase synthesis, utilizing organic solvents to produce fine particles, offers scalability and cost-effectiveness compared to high-temperature solid-state reactions [68,69].

Sulfide SSEs have gained significant research interest owing to their ultrahigh ionic conductivity [67]. However, challenges such as interfacial instability, electrode architecture optimization, and scalable manufacturing processes hinder their practical applications [70] Recent advancements in material science and engineering have positioned sulfide SSEs as critical enablers for next-generation ASSBs. Their remarkable ionic conductivity, with intrinsic electrochemical stability and robust safety profiles, make them critical for developing high-energy-density and inherently safe battery systems. Consequently, sulfide-based ASSBs are poised for transformative applications in portable electronics and grid-scale energy storage, where energy density and operational safety are crucial.

1.2. Significance of Research on Sulfide SSEs

Sulfide SSEs are regarded as an essential technology for ASSBs due to their exceptional ionic conductivity, mechanical ductility, and stable interfacial compatibility with electrodes [71]. Notably, lithium-ion conductors such as LGPS exhibit ultrahigh ionic conductivities (>10^{-2} S·cm^{-1} at 25 °C) [57], approaching those of liquid electrolytes. Solid Power Semiconductor and SVOLT Energy Technology Co., Ltd. (Changzhou, China) have successfully developed 20 Ah sulfide-based ASSBs. Meanwhile, Mitsui Mining & Smelting Co., Ltd. (1-11-1, Oosaki, Shinagawa-ku, Tokyo, Japan) and Pohang Iron and Steel Co., Ltd. (Pohang, Republic of Korea) have established pilot production lines for sulfide-based solid-state electrolytes (SSEs). Additionally, Solid Power (Louisville, CO, USA), Samsung Electronics (Shenzhen, China), and Nissan Motor Co., Ltd. (1-1-1, Takashima, Nishi-ku, Yokohama, Japan) have initiated the construction of pilot production lines for sulfide-based ASSBs [72].

As shown in Figure 2, despite these achievements, the full-scale commercialization of sulfide-based ASSBs remains hindered by critical challenges: material instability, electrode limitations, interfacial failure, and composite electrode optimization.

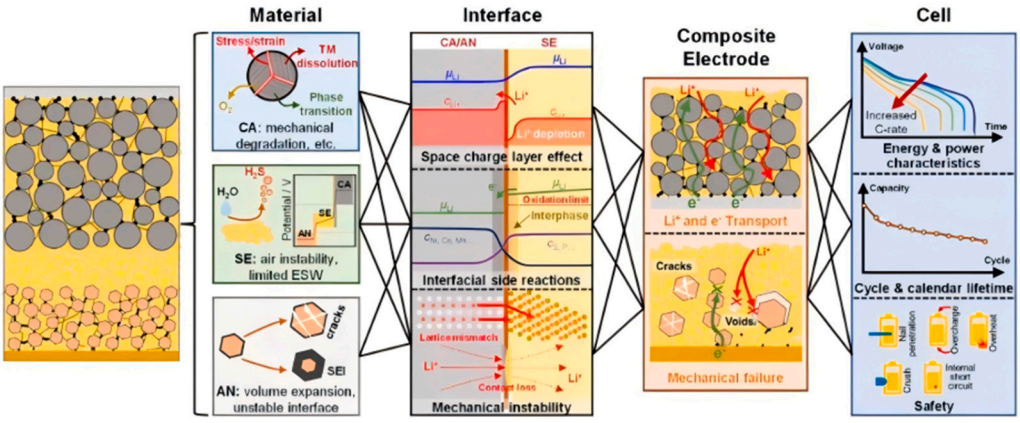


Figure 2. Challenges for sulfide-based ASSBs: from materials, interfaces, and composite electrodes to battery [72]. Reproduced with permission from Ref. [72]. Copyright 2023, Elsevier.

Material instability: Sulfide SSEs suffer from poor air stability and narrow electrochemical stability windows (ESWs) [73,74]. For instance, LGPS demonstrates high ionic conductivity but reacts aggressively with lithium metal anodes. Wet-chemical synthesis and particle size optimization (e.g., via ball milling) are being explored to enhance air stability and ionic transport [74].

Electrode limitations: High-voltage cathodes (e.g., Ni-rich NCM, and Li-rich layered oxides) and silicon/lithium anodes enable high energy density but face structural degradation during cycling [54,56]. Microstructure engineering and doping strategies are critical to mitigate mechanical fracture [56].

Interfacial failure: Space charge layer (SCL) formation, interfacial side reactions, and mechanical stress disrupt Li^+ transport at electrode–electrolyte interfaces. Buffer layers (e.g., cathode coatings and artificial SEI layers) and hybrid electrolyte designs show promise, yet achieving uniformity at scale remains challenging [75,76].

Composite electrode optimization: Inhomogeneous distributions of active materials, SSEs, and conductive additives in composite electrodes impede ion/electron transport. Mechanical failures (e.g., particle cracking and pore formation) exacerbate dendrite growth. Applied pressure during cell assembly alleviates these issues, but optimal pressure parameters require further study [77,78].

Addressing these challenges—material instability, interfacial failure, electrode design limitations, and scalable manufacturing—will unlock the full potential of sulfide-based ASSBs. With continued innovation, these systems are poised to revolutionize energy storage for electric vehicles, portable electronics, and grid-scale applications, offering superior energy density and safety [79].

2. Properties of Sulfide SSEs

2.1. Types and Chemical Compositions of Sulfide SSEs

Sulfide SSEs exhibit exceptional lithium-ion conductivity and mechanical properties, surpassing polymer-based and oxide-based SSEs [80]. Based on crystallinity, sulfide SSEs are categorized into three classes: amorphous (glassy), glass–ceramic, and crystalline [81].

2.1.1. Glassy Sulfide SSEs

Glassy sulfide SSEs are typically synthesized by melting stoichiometric mixtures of Li_2S and P_2S_5 at temperatures exceeding 900 °C, followed by rapid quenching to inhibit crystallization. The absence of grain boundaries in amorphous structures eliminates interfacial resistance, enabling isotropic Li^+ transport. The binary system $xLi_2S{\cdot}(100 - x)P_2S_5$ ($40 \leq x \leq 80$) is the most studied, with ionic conductivity following an Arrhenius temperature dependence, indicating thermally activated Li^+ migration [82].

Strategies to enhance conductivity include [83] high-energy ball milling to induce disordered structures by bond disruption; melt quenching for rapid glassy-phase formation that enhances atomic mobility; and anion doping (e.g., O^{2-} or Cl^- for S^{2-}) to optimize Li^+ pathways via lattice modification. These concerted multiscale engineering strategies address ion transport barriers across atomic and microstructural scales.

2.1.2. Glass–Ceramic Sulfide SSEs

When glassy sulfide electrolytes undergo complete crystallization, they typically exhibit reduced ionic conductivity. This is due to structural reorganization during crystallization, which disrupts ion transport pathways. However, certain glass–ceramic electrolytes demonstrate higher ionic conductivity than their fully amorphous or crystalline counterparts, rendering them particularly advantageous in specific applications.

The high-temperature crystallization process enables the transformation of glassy sulfides into glass–ceramic electrolytes by partially retaining amorphous domains while introducing crystalline phases [84]. This dual-phase structure–combining amorphous and crystalline regions–alters atomic arrangements and chemical bonding at the microscale, critically influencing ionic conduction [85].

Within glass–ceramic sulfide electrolyte research, the Li_2S-P_2S_5 system remains predominant due to its tunable ionic conductivity and chemical stability [86]. Annealing temperature plays an important role: higher temperatures accelerate ion migration and lattice vibrations, thereby enhancing conductivity [87]. For example, J. Kim et al. annealed $78Li_2S$-$22P_2S_5$ glass at 160 °C and 260 °C, respectively [88]. At 160 °C, microcrystalline

nucleation occurred, yielding a room-temperature conductivity of 4.5×10^{-4} S·cm^{-1} [88]. Subsequent annealing at 260 °C promoted grain growth, forming a thio-LISICON phase with conductivity reaching 8.5×10^{-4} S·cm^{-1} [88]. These results demonstrate that controlled crystallization optimizes microstructural and macroscopic properties, balancing amorphous flexibility with crystalline ionic pathways.

2.1.3. Crystalline Sulfide SSEs

Among crystalline sulfide SSEs, thio-LISICON and argyrodite electrolytes have emerged as prominent candidates due to their unique ionic conduction mechanisms [89]. The thio-LISICON family, derived by substituting sulfur for oxygen in oxide LISICON structures (e.g., γ-Li_3PO_4), adopts the general formula $Li_{4-x}A_{1-\gamma}B_\gamma S_4$ (A = Si, Ge; B = Zn, Al, P) [90]. For instance, the interaction between Li_6PS_5Cl(LSPC) and polar PVDF-TrFE ensures a high lithium-ion conductivity (≈1.2 ms/cm) at room temperature and good mechanical ductility of the composite electrolyte membrane [91]. However, its poor compatibility with lithium metal and the high cost of germanium limits practical applications. To address this, SnS_2 and SiS_2 substitutions have been explored. Y. Kato et al. synthesized $Li_{9.54}Si_{1.74}P_{1.44}S_{11.7}Cl_{0.3}$ (25 ms/cm) via solid-state methods, and it exhibited twice the conductivity of LGPS and superior cycling stability [23]. In ASSBs employing $LiNi_{0.83}Mn_{0.06}Co_{0.11}O_2$ (NMC811) cathodes, this SSE maintains 92% capacity retention after 1000 cycles at 1.0 mA·cm^{-2}, even under high humidity [92].

Argyrodite is named after the mineral Ag_8GeS_6, whose high ionic conductivity in silver and germanium ions inspired its adaptation as a structural template for designing fast lithium-ion conductors. Among argyrodite-type electrolytes, Li_6PS_5X (X is Cl, Br, I, etc.) has garnered the most extensive research attention due to its superior ionic transport properties [93]. H. J. Deiseroth et al. pioneered the discovery of Li_6PS_5X, a lithium-ion conductor derived from the Ag_8GeS_6 framework, which stabilizes the high-temperature phase of Li_7PS_6 at room temperature [24]. The crystal structure of Li_6PS_5X (cubic F-43 m space group) features halogen atoms (X) at cube vertices and face centers, PS_4 tetrahedra at edge midpoints, and lithium ions dynamically occupying 18 sites, forming a 3D conduction network [94].

S. J. Liu et al. developed a flexible composite SSE membrane through a sequential process of electrospinning, solution perfusion, and hot pressing. The resulting membrane, with a thickness of 30–40 μm, integrates LSPC particles within a polar PVDF-TrFE [95]. Strong interfacial interactions between the polar PVDF-TrFE framework and LSPC endow the composite with high mechanical ductility and a room-temperature Li^+ conductivity of 1.2×10^{-3} S·cm^{-1} [95]. When incorporated into a button-type ASSB configuration—featuring an $LiNi_{0.8}Co_{0.1}Mn_{0.1}O_2$ (NCM811) cathode and lithium–indium alloy anode—the membrane demonstrated exceptional cycling stability. At a current density of 1.0 mA/cm^2 within a voltage window of 2.5–4.3 V, the ASSB retained 92% capacity after 1000 cycles and 71% after 20,000 cycles, indicating its potential for long-term applications [91].

2.2. Physical and Chemical Properties

2.2.1. Ionic Conductivity

The ionic conductivity of an SSE is a key determinant of Li^+ ion mobility and serves as a critical performance metric for evaluating its suitability in practical applications. Sulfide SSEs exhibit superior ionic conductivity compared to oxide and polymer counterparts due to sulfur's larger atomic radius, lower electronegativity, and reduced Li^+ binding energy. For instance, the ionic conductivity of LGPS is 1.2×10^{-2} S·cm^{-1}, and that of $Li_{9.54}Si_{1.74}P_{1.44}S_{11.7}Cl_{0.3}$ is 2.5×10^{-2} S·cm^{-1} [23]. High ionic conductivity can reduce the internal resistance of the battery, and improve the electrochemical properties [96].

Sulfide SSEs are typically prepared by melting stoichiometric mixtures (e.g., Li_2S and P_2S_5) at high temperatures (>900 °C) under argon, followed by rapid quenching to form amorphous phases. For glass–ceramic electrolytes, controlled crystallization is subsequently induced [97].

The melt synthesis of sulfide solid-state electrolytes typically follows a three-stage procedure to ensure reliable ionic conductivity measurements [98]. Initially, precursor powders with controlled stoichiometry are prepared through either pre-synthesized spheroidal particles or mechanically milled raw materials. These homogenized mixtures are subsequently compressed under controlled pressure (typically 300–500 MPa) to form densified pellets with minimized porosity. The final consolidation involves encapsulating the compacted specimens in vacuum-sealed quartz ampoules under argon atmosphere, a critical step for preventing sulfur volatilization and oxide contamination during high-temperature processing. This standardized protocol enables a reproducible fabrication of SSE samples suitable for electrochemical characterization [98].

After calcination at high temperature, the mixture is rapidly cooled to achieve rapid quenching, thus obtaining a glassy sulfide electrolyte. If it is necessary to prepare a glass–ceramic electrolyte, it can be achieved by further crystallization. F. Mizuno et al. demonstrated that increasing the melting temperature from 750 °C to 900 °C enhances the formation of $P_2S_6^{4-}$ units in $70Li_2S$-$30P_2S_5$ ($Li_7P_3S_{11}$), significantly boosting ionic conductivity [99]. Y. Seino et al. further optimized this process through hot pressing, achieving 1.7×10^{-2} S·cm^{-1} by reducing grain boundary resistance [25].

Glassy sulfide electrolytes exhibit intricate local structures influenced by Li_2S content [36]. Dietrich et al. demonstrated that the composition of $xLi_2S{\cdot}(100 - x)P_2S_5$ glass varies with the Li_2S content [100]. When the Li_2S content is low ($x \leq 60$), the glassy sulfide electrolyte is mainly composed of corner-sharing tetrahedra $P_2S_7^{4-}$ units, each containing one bridging S atom and three terminal S atoms. Glassy sulfide electrolytes with higher Li_2S content ($x \geq 70$) contain more isolated tetrahedral PS_4^{3-} units, where all S atoms are terminal [100]. Among all glassy sulfide electrolytes, $75Li_2S{\cdot}25P_2S_5$ has the highest ionic conductivity at room temperature [36].

2.2.2. Mechanical Strength

Lithium dendrite penetration remains a critical challenge at the lithium metal–SSE interface, despite the higher mechanical strength of sulfide SSEs compared to lithium metal [100]. Dendrites tend to nucleate preferentially at material defects, such as grain boundaries and cracks, and can propagate even in amorphous sulfide electrolytes that lack crystalline interfaces [101,102]. For instance, M. Nagao et al. observed lithium dendrite growth along grain boundaries in polycrystalline SSEs and within bulk regions of glassy sulfides [102].

On the other hand, the interface between the SSE and lithium metal experiences significant strain and uneven current density during cycling, primarily due to volume expansion and non-uniform lithium deposition/dissolution. These issues are largely attributed to poor interfacial contact. Regions with localized high current density are known to facilitate the nucleation and growth of lithium dendrites [103]. The study of lithium electrodeposition on the single crystal $Li_6La_3ZrTaO_{12}$ garnet shows that to reduce the penetration of lithium through the brittle electrolyte, the interface defects between the SSE and the lithium metal should be minimized [104].

In ASSBs, the volume changes of the lithium metal anode during Li deposition and dissolution induce significant structural stress at the electrode–electrolyte interface. Therefore, the design of the SSE–electrode interface must account for and endure cyclic mechanical stresses during battery operation [105]. Electrochemical reactions in ASSBs occur at the solid–solid interface between the electrolyte and electrode, requiring specialized engineer-

ing to achieve optimal interfacial contact and efficient ion–electron transport [106]. To engineer these challenges, it is essential to reduce interfacial impedance by minimizing resistance caused by physical contact defects and poor interfacial adhesion [90]. Additionally, the mechanical compatibility of sulfide-based SSEs must be ensured, leveraging their lower elastic modulus (e.g., (18.5 ± 0.9) GPa for $70Li_2S$-$30P_2S_5$) to achieve compliant contact and accommodate interfacial stress mismatches [107].

However, sulfide SSEs face trade-offs between flexibility and brittleness. Their fracture toughness (0.23 ± 0.04 MPa·$m^{1/2}$) and hardness (1.9 ± 0.2 GPa) are considerably lower than those of oxide-based electrolytes, rendering them prone to defect propagation during cycling [107]. Resolving these issues demands a deeper understanding of sulfide SSE mechanics to balance ionic conductivity, interfacial stability, and mechanical robustness [108–110].

2.2.3. Thermal and Electrochemical Stability

Most highly conductive sulfide SSEs (e.g., LGPS, $Li_7P_3S_{11}$, and $Li_{9.54}Si_{1.74}P_{1.44}S_{11.7}Cl_{0.3}$) exhibit thermodynamic instability when in contact with lithium metal. Wenzel et al. classified the interfacial stability into three categories [111].

Thermodynamically stable interfaces: SSE and Li metal coexist in equilibrium without reactive decomposition [112]. Unstable interfaces with mixed conduction: electron/ion-conducting interphases form, enabling continuous electrolyte degradation and rapid capacity fade [113]. Passivating interfaces: electrically insulating but ion-conductive layers (analogous to liquid electrolyte-derived SEI) prevent further side reactions [111].

The narrow ESW of sulfide SSE limits compatibility with conventional electrodes operating beyond their stability limits [114]. To achieve stable cycling in ASSBs, engineered interphases must be designed to fulfill multiple functions simultaneously: passivation to suppress electrolyte decomposition; high ionic conductivity to minimize interfacial impedance; and electron insulation to prevent undesirable side reactions. For instance, electron-insulating interphases (e.g., Li_3P and Li_2S) can effectively passivate sulfide-based SSEs, thereby preserving cycling stability. Conversely, mixed-conductor interphases, which facilitate concurrent ion and electron transport, may drive thermodynamically favored electrolyte decomposition, leading to progressive interface thickening, increased impedance, and accelerated performance degradation [115–123].

Interface engineering strategies primarily utilize buffer layers (e.g., $LiNbO_3$ and Li_3PO_4) inserted between electrodes and sulfide-based SSEs to address interfacial challenges. These buffer layers reduce interfacial resistance by improving physical contact, inhibit electron transfer to prevent detrimental side reactions, and enhance air stability through moisture and oxygen shielding, thereby maintaining the structural and chemical integrity of sulfide SSEs [36]. Such advancements highlight the important role of tailored interfacial design in enabling robust sulfide-based all-solid-state lithium batteries with extended cycle life and operational reliability [117].

2.3. Ionic Conduction Mechanism of Sulfide SSEs

2.3.1. Thio-LISICON Mechanism

Thio-LISICON structures, first identified in Li_2S-GeS_2, Li_2S-GeS_2-Ga_2S_3, and Li_2S-GeS_2-ZnS systems, are derived from the γ-Li_3PO_4-type oxide LISICON framework by substituting oxygen with sulfur. The lower electronegativity and larger ionic radius of sulfur reduce Li^+ binding energy, widening ion migration channels and enabling higher ionic conductivity compared to oxide analogues [118].

These materials adopt an orthorhombic *Pnma* crystal structure, where S^{2-} ions form hexagonally close-packed arrays. Heavy metal cations (e.g., Ge^{4+} and Zn^{2+}) occupy tetrahedral sites, while Li^+ ions reside in disordered octahedral interstices. Representative

compounds include Li_4GeS_4 (2.0×10^{-7} S·cm^{-1}) and Li_4SnS_4 (7.0×10^{-5} S·cm^{-1}), though their intrinsic conductivity remains insufficient for practical applications [119].

Aliovalent cationic doping (e.g., P^{5+} or Al^{3+} substitution for Si^{4+} in Li_4SiS_4) enhances ionic conductivity by introducing Li vacancies or interstitials, thereby optimizing percolative ion transport pathways. For instance, $Li_{3.4}Si_{0.4}P_{0.6}S_4$: P^{5+} doping creates Li vacancies, elevating to 6.7×10^{-4} S·cm^{-1} at 27 °C [124]. ($Li_{4.8}Si_{0.2}Al_{0.8}S_4$: Al^{3+} substitution generates Li interstitials, elevating to 2.3×10^{-7} S·cm^{-1}) [124].

2.3.2. Structure Mechanism of $Li_{11-x}M_{2-x}P_{1+x}S_{12}$ (M = Ge, Sn, Si)

The $Li_{11-x}M_{2-x}P_{1+x}S_{12}$ (M = Ge, Sn, Si) exemplifies how atomic-scale structural engineering enhances ionic transport. In LGPS, the crystal framework comprises interconnected chains of ($Ge_{0.5}P_{0.5}$) S_4 tetrahedra and LiS_6 octahedra, forming 1D Li^+ diffusion channels along the c-axis [123]. These channels are bridged by LiS_4 tetrahedra, creating a hierarchical conduction network. The density functional theory (DFT) calculations reveal ultra-low activation energies for Li^+ migration: 0.17 eV for interplanar hopping between ab-plane and tetrahedral sites, 0.18 eV for intra-channel (c-axis) migration, and 0.37 eV for pure ab-plane diffusion [123]. This anisotropic energy landscape enables rapid Li^+ transport, even with partial channel obstruction, by leveraging low-barrier interplanar pathways, thus underpinning the exceptional ionic conductivity of LGPS [123].

The anionic substitution of S with O in $Li_{10}MP_2O_{12}$ (M = Ge or Si) enhances redox stability but compromises ionic conductivity due to tightened Li^+ migration channels, raising activation energy to 0.36 eV and reducing to 3.0×10^{-5} S·cm^{-1} [125]. However, partial O substitution ($0 \leq x<0.9$) retains the parent P42/nmc space group while improving electrochemical resilience [125]. For instance, $Li_{9.42}Si_{1.02}P_{2.1}S_{9.96}O_{2.04}$ maintains a moderate 3.2×10^{-4} S·cm^{-1} alongside enhanced stability, demonstrating the viability of controlled anionic doping to balance ionic transport and interfacial durability in sulfide SSEs [126].

Halogen substitution (e.g., Cl^- and I^-) in sulfide electrolytes enhances Li^+ mobility by reducing anion–Li^+ electrostatic interactions and expanding ionic diffusion channels. In $Li_{9.54}Si_{1.74}P_{1.44}S_{11.7}Cl_{0.3}$, Cl^- incorporation facilitates three-dimensional (3D) Li^+ diffusion through 16h/8f/4c interstitial sites, achieving 2.5×10^{-2} S·cm^{-1} at room temperature [127]. Iodine's larger ionic radius and lower electronegativity further widen channels, enabling lower migration barriers. This is exemplified by $Li_{9.54}Si_{1.74}P_{1.44}S_{11.7}Cl_{0.3}$, which achieves an ionic conductivity of 1.35×10^{-3} S·cm^{-1} at room temperature through iodine doping, demonstrating that halogen size and electronic properties critically govern channel dimensions and Li^+ transport efficiency in sulfide SSEs [128].

2.3.3. Ionic Conduction Mechanism in Li_6PS_5X (X = Cl, Br and I) Argyrodites

The Li_7PS_6 system exists in two phases: a high-temperature phase (HT-Li_7PS_6, 3.0×10^{-5} S·cm^{-1}) and a low-temperature phase (LT-Li_7PS_6, 1.6×10^{-6} S·cm^{-1}), both exhibiting limited ionic conductivity. In contrast, the Li_6PS_5X (X = Cl, Br, I) argyrodite family adopts a cubic F-43 m structure, where S^{2-} and X^- anions occupy face-centered 4a/4d sites, while PS_4^{3-} tetrahedra reside at octahedral positions (P at the 4b positions) [129]. Sulfur anions fully occupy 16e sites, whereas S^{2-} and X^- share 4a/4b sites, creating a dynamically disordered Li^+ migration network [129].

The Li^+ transport dynamics in Li_6PS_5X involve three cooperative mechanisms: short-range intra-cage hopping between adjacent 48 h sites; inter-cage transitions within tetrahedral subunits; and long-range inter-cage diffusion across adjacent units. The rate-limiting step is typically governed by the slowest process, which is often long-range diffusion. The introduction of Li^+ vacancies through halogen substitution (e.g., Cl^- replacing S^{2-} in Li_7PS_6) significantly enhances ionic conductivity. For example, Li_6PS_5Cl and Li_6PS_5Br

achieve conductivities of ~10^{-2} S·cm^{-1} at 25 °C, whereas Li_6PS_5I exhibits a lower conductivity of ~10^{-5} S·cm^{-1} due to the larger ionic radius of iodide, which induces lattice distortion and steric hindrance to Li^+ migration [101].

Doping strategies significantly enhance the ionic conductivity of sulfide SSEs by tailoring their atomic-scale structure and defect chemistry. The partial substitution of S^{2-} and I^- in $Li_{7-x}PS_{6-x}I_x$ introduces interstitial sites that enable 3D Li^+ percolation, achieving optimal conductivity at $0.75 \leq x \leq 0.95$, the Li^+ due to a balanced vacancy–interstitial distribution [128]. Similarly, Si^{4+} doping in $Li_{6+x}P_{1-x}Si_xS_5Br$ (x = 0.35–0.5) expands Li^+ migration channels through lattice parameter enlargement and carrier concentration elevation, tripling the ionic conductivity compared to undoped Li_6PS_5Br. This performance enhancement is predominantly governed by reduced activation barriers and enhanced Li^+ mobility across widened diffusion pathways [86]. These doping strategies underscore the intricate relationship between cationic/anionic substitution, lattice dynamics, and ionic transport efficiency in sulfide-based electrolytes [86].

3. Synthesis Methods for Sulfide SSEs

The synthesis of sulfide-based SSEs is typically carried out under inert atmospheres to prevent moisture-induced degradation, and the resulting materials are categorized into glassy, glass–ceramic, and crystalline states based on their structural order [130–133]. Key synthesis routes include mechanical ball milling, high-temperature solid-state reactions, and liquid-phase synthesis, each offering distinct advantages in optimizing ionic conductivity and interfacial compatibility [134].

3.1. Mechanical Ball Milling

Mechanical ball milling involves blending stoichiometric precursors (e.g., Li_2S, P_2S_5, and LiCl) in a ball mill with grinding balls, followed by controlled milling to induce amorphous-to-crystalline phase transitions. For instance, LPSC argyrodite was synthesized by milling at 300 rpm for 8 h, achieving 4.049×10^{-3} S·cm^{-1} after sintering at 500 °C [135–137]. Prolonged milling enhances particle refinement and amorphous phase formation, while excessive sintering temperatures (>500 °C) risk crystal structure degradation.

Liu et al. demonstrated that $70Li_2S - (30 - x)P_2S_5_xCe_2S_3$ (x = 0, 0.5, 1, 2, 3) glass–ceramic, prepared via high-energy ball milling and heat treatment, exhibits 1.52×10^{-3} S·cm^{-1} at 25–40 °C higher than undoped $70Li_2S$-$29P_2S_5$-Ce_2S_3. ASSBs incorporating this electrolyte delivered a 105.3 mAh·g^{-1} initial capacity at 0.1 °C, retaining 87.2% after 50 cycles [138].

3.2. High-Temperature Solid-State Reaction

Solid-state reactions at elevated temperatures (e.g., 750 °C to 900 °C) promote the formation of conductive phases like $Li_7P_3S_{11}$. Mizuno et al. showed that increasing the melting temperature from 750 °C to 900 °C enhances $P_2S_6^{4-}$ unit formation, boosting ionic conductivity by 50% due to optimized Li^+ percolation pathways [139–141].

3.3. Liquid-Phase Synthesis

Liquid-phase synthesis dissolves metal salts (e.g., Li_2S and P_2S_5) in solvents like tetrahydrofuran (THF), followed by precipitation or evaporation to yield nanostructured SSEs. Liu et al. synthesized β-Li_3PS_4-containing glass–ceramic via THF-mediated routes, achieving 1×10^{-4} S·cm^{-1} at room temperature after crystallization [142–148].

4. Synthesis and Application Strategies for Sulfide SSEs

Sulfide SSEs have emerged as a cornerstone technology for next-generation ASSBs, driven by their ultrahigh ionic conductivity (>1 × 10^{-3} S·cm^{-1}) and exceptional mechanical flexibility. These attributes enable seamless integration with high-capacity electrodes like silicon and lithium metal, addressing key challenges in energy density (>400 Wh/kg) and safety for applications in electric vehicles and portable electronics [149–154].

The structural and ionic advantages of sulfide-based solid-state electrolytes (SSEs) arise from the replacement of oxygen with sulfur in oxide-derived frameworks. The lower electronegativity of sulfur (2.58 compared to 3.44 for oxygen) weakens the interaction between Li^+ and anions, while its larger ionic radius (1.84 Å versus 1.40 Å for O^{2-}) expands the Li^+ migration pathways. These combined effects facilitate ultrafast ionic transport [12,24]. These properties have driven landmark advancements, such as the 2011 synthesis of LGPS with a room-temperature conductivity of 1.2 × 10^{-2} S·cm^{-1}, and the 2016 development of $Li_{9.54}Si_{1.74}P_{1.44}S_{11.7}Cl$, which achieved 2.5 × 10^{-2} S·cm^{-1}—performance rivaling conventional liquid electrolytes [24].

Sulfide-based SSEs effectively address the 300% volume expansion of silicon anodes through several mechanisms: rapid Li^+ diffusion (D ~ 10^{-8} cm^2·s^{-1}), which homogenizes electrochemical reactions [72]; elastic buffering (Young's modulus: 18.5 GPa), which reduces interfacial stress [155]; and the application of external pressure (1–10 MPa), which maintains electrode–electrolyte contact and lowers impedance by up to 50% [156,157].

The higher lithiation potential of silicon (0.4 V vs. Li^+/Li) compared to graphite (0.1 V) further inhibits electrolyte decomposition, enabling stable operation at voltages up to 4.3 V [158–160]. Prototype ASSBs incorporating silicon anodes and sulfide-based SSEs achieve energy densities exceeding 300 Wh/kg, even with electrolyte layers as thin as 50 µm [161].

The development of $Li_7P_3S_{7.5}O_{3.5}$ (LPSO) represents a significant advancement in cost-effective sulfide-based SSEs, as illustrated in Figure 3a,b. This material combines an ultra-low density (1.70 g·cm^{-3}, 32% lower than halides), competitive raw material costs ($14.42/kg, less than 8% of conventional sulfide SSEs), and robust electrochemical performance [158–160]. Synthesized from low-cost hydrated lithium hydroxide and phosphorus sulfide, LPSO retains 89.29% capacity after 200 cycles at 60 °C in Figure 3c,d. As shown in Figure 3e, the symmetrical battery composed of LPSO and lithium metal can achieve a stable cycle of more than 4200 h at room temperature, and its production cost aligns with industrial targets (<$50/kg), positioning it as a frontrunner for scalable, high-performance ASSBs [161].

Sc_2O_3 doping (4 mol%) elevates ionic conductivity to 3.17 × 10^{-2} S·cm^{-1} at room temperature while enabling 300 h stable Li–Li symmetric cell cycling at 0.1 mA/cm^2 [162–164]. Thin-film processing via roll pressing (e.g., $Li_{5.4}PS_{4.4}C_{l1.6}$/PTFE) yields 30 µm membranes with 8.4 mS·cm^{-1}, delivering a 135.3 mAh·g^{-1} (1.4 mAh·cm^{-2}) capacity and 80.2% retention over 150 cycles in NCM-based ASSBs [165].

Despite significant advancements in air stability (achieved through rare-earth doping) and interfacial passivation (enabled by artificial SEI layers), sulfide-based SSEs still face several challenges: enhanced moisture resistance, requiring handling protocols under relative humidity (RH) < 1%; improved compatibility with lithium metal, targeting critical current densities exceeding 1 mA·cm^{-2}; and scalable manufacturing processes capable of producing films thinner than 50 µm to enable energy densities surpassing 400 Wh/kg [166]. Addressing these interconnected challenges, which encompass material stability, interfacial kinetics, and industrial process engineering, will play a decisive role in determining the viability of sulfide-based SSEs in next-generation ASSBs [167,168].

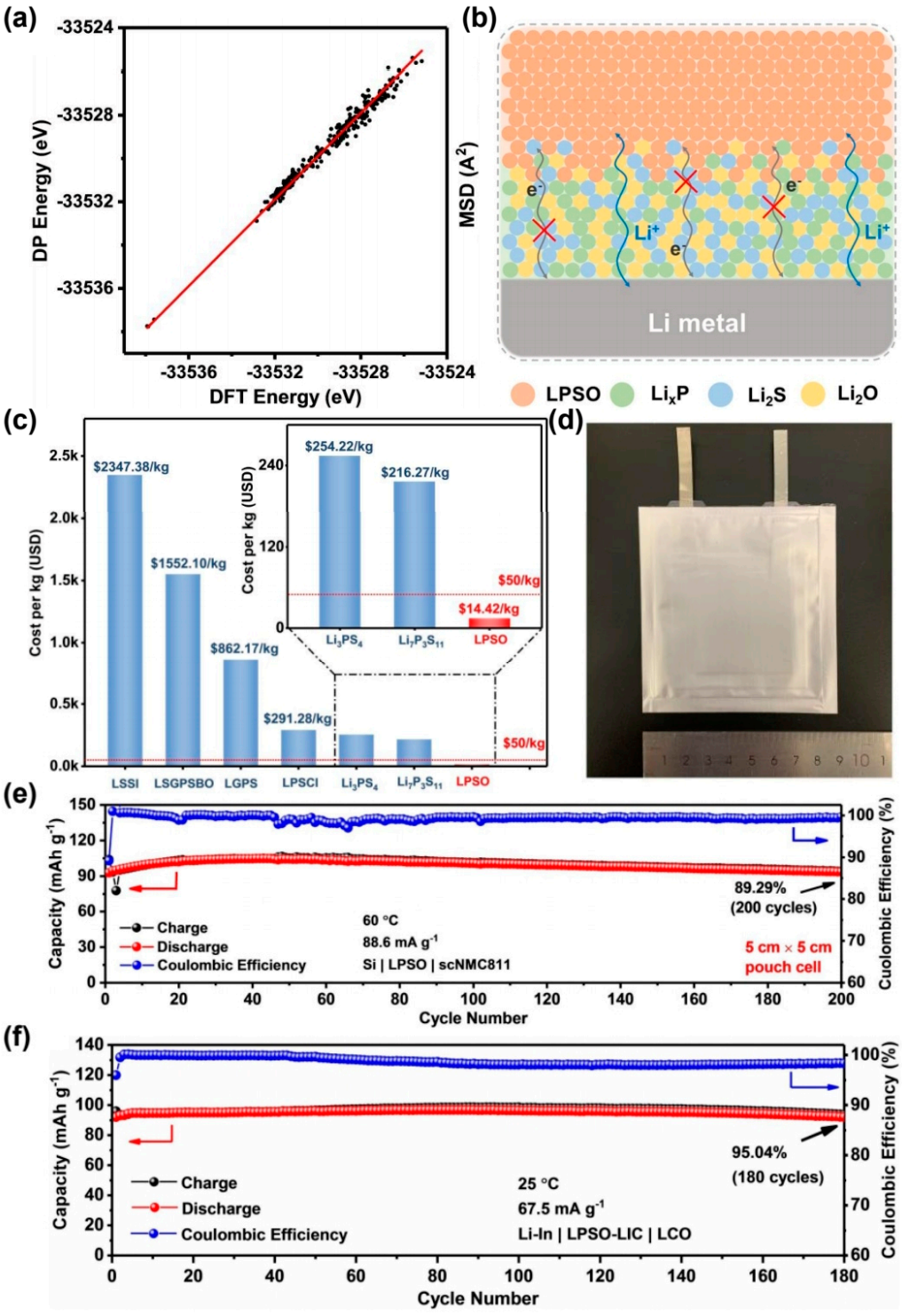


Figure 3. (**a**,**b**) Comparison of deep learning potential and DFT energy for P1 crystal phase of LPSO. These points are calculated data points, the red line is a linear fit, a diagram of the interface behavior between LPSO and Li metals [157]; (**c**) raw material costs for LPSO and other widely studied sulfide SSEs [157]; (**d**) physical batteries composed of LPSO with silicon and nickel [157]; (**e**) Long-term cycling performance of Si | LI | scNMC811 at 88.6 m·Ag [157]; (**f**) Liin | lpso-lic | LCO at 67.5 m·Ag [157]. (**a**–**f**) Reprinted with permission from ref. [157]. Copyright 2024, Wiley-VCH.

5. Challenges and Solutions for Sulfide SSEs

Sulfide-based SSEs have become key materials for advancing ASSBs due to their superior ionic conductivity and mechanical flexibility compared to oxide and halide alter-

natives. However, their practical application is hindered by significant challenges, such as interfacial instability, air sensitivity, and high production costs. Overcoming these obstacles demands a thorough understanding of material properties, interfacial behavior, and scalable synthesis approaches.

5.1. Interface Stability of Sulfide SSEs

Sulfide-based SSEs are critical for enabling high-performance ASSBs. However, their practical application is limited by interfacial instability caused by inherent material constraints. The narrow electrochemical stability window (ESW) of sulfide SSEs (1.6–2.3 V vs. Li^+/Li) triggers detrimental side reactions at high-voltage cathode interfaces, such as $LiCoO_2$ (LCO), leading to the formation of resistive space charge layers (SCLs), as illustrated in Figure 4 [54,55]. These layers form as a result of lithium-ion depletion within the sulfide-based SSE and simultaneous enrichment at the cathode during cycling, driven by gradients in chemical potential. For instance, LSPC exhibits a room-temperature conductivity of 2.5×10^{-2} S·cm^{-1} at room temperature, but its utility is curtailed by interfacial reactions that increase impedance and degrade cycle stability [57].

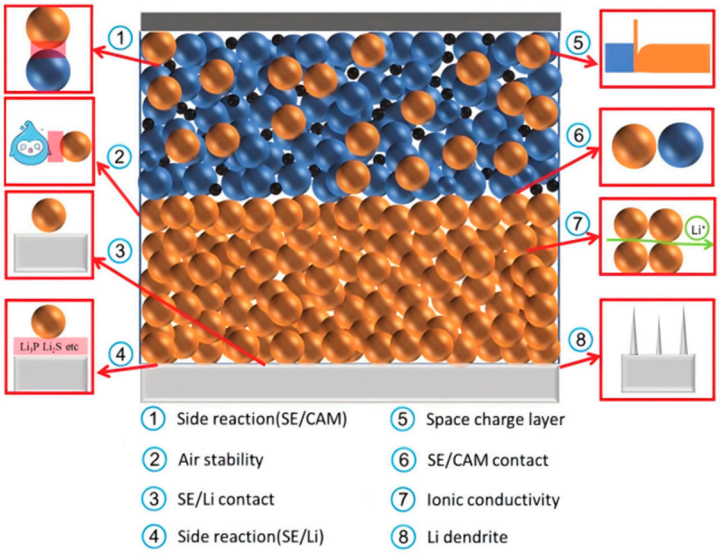


Figure 4. Problems of sulfide-based ASSBs; for the cathode electrode–electrolyte interface, there are mainly side reactions and SCLs. For the sulfide electrolyte, the main improvement is ion conductivity and air stability. The anode electrode–electrolyte interface is mainly an interfacial side reaction and lithium dendrites [54]. Reprinted with permission from Ref. [54]. Copyright 2023, Elsevier.

The formation and evolution of SCLs are further illustrated in Figure 5, and as shown in Figure 5a, similar to the charging voltage curve of a capacitor. At the onset of cell polarization, lithium ions migrate from the sulfide SSE to the anode, while cathode delithiation is delayed until the interfacial potential exceeds the cathode's redox threshold in Figure 5b–d. This asymmetry thickens the Li^+-depleted region in the SSE, amplifying interfacial resistance. Even after cathode delithiation compensates for the depletion layer in Figure 5d, residual impedance persists, underscoring the need for mitigation strategies such as buffer layers or electric field modulation [169–177].

As shown in Figure 6a,b, interfacial side reactions exacerbate degradation. At the cathode, sulfide SSEs oxidize to form low-conductivity phases (e.g., sulfates and polysulfides), while anode-side reduction generates electronically conductive interphases that accelerate electrolyte decomposition.

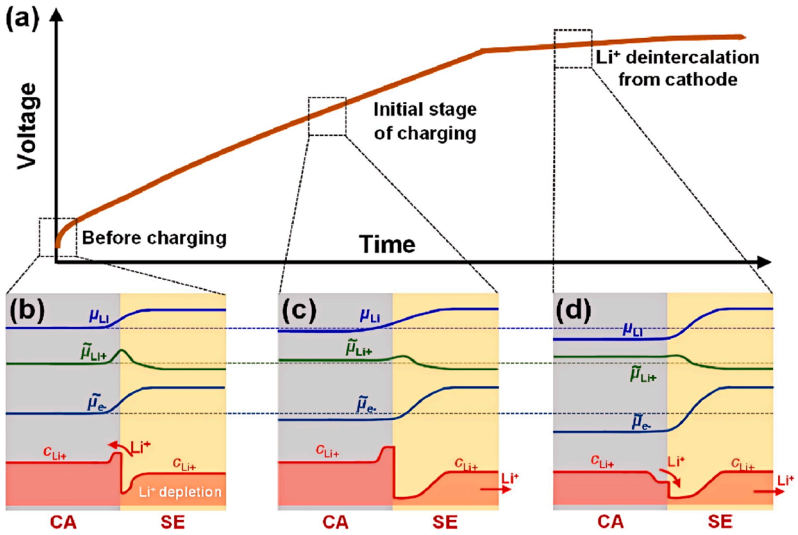


Figure 5. Evolution of the SCL at the cathode CA | SE interface and its solution [72]. (**a**–**d**) Schematic diagram of SCL formation and evolution during charging [175–177]. (**a**–**d**) Reprinted with permission from Ref. [72]. Copyright 2023, Elsevier.

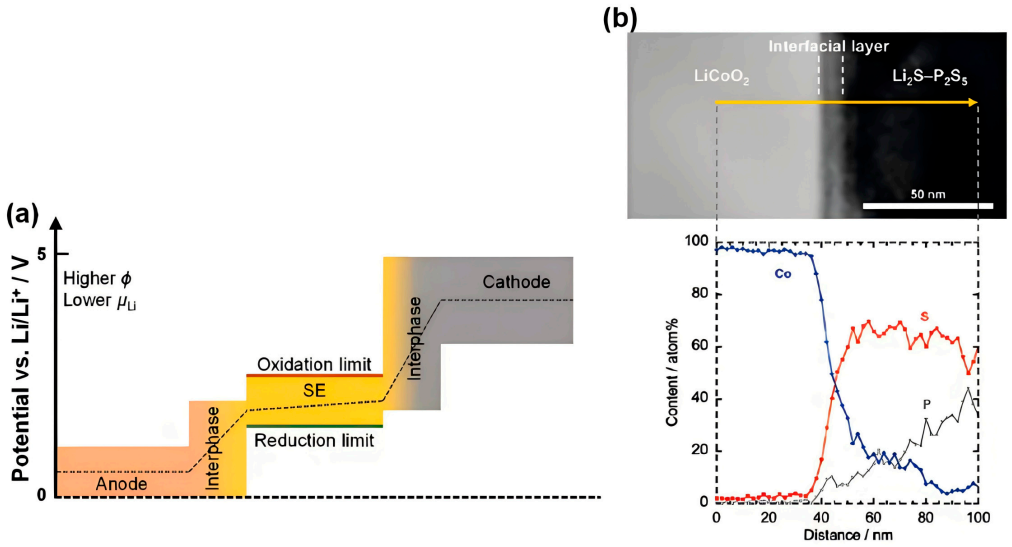


Figure 6. Interface reaction between electrode and sulfide SE [72]. (**a**) Schematic diagram of electrochemical side reactions at the interface of CA | SE and AN | SE [178]. (**b**) Interface characterization and mutual diffusion of Co, P, and S elements on LCO | Li_2S-P_2S_5 interface [179]. Reprinted with permission from Ref. [72]. Copyright 2023, Elsevier.

These reactions release gases like SO_2 and create mixed ion–electron-conductive interfaces, further destabilizing ASSBs [180–184]. Coating strategies, such as the 6.3 nm $LiNbO_3$ layer on NCM811 cathodes in Figure 7a,b, physically isolate the cathode from the SSE, reducing interfacial impedance by 50% and enhancing cycling stability [178]. Ideal coatings must balance ionic conductivity, electronic insulation, and mechanical resilience to accommodate volume changes during lithiation/delithiation [178].

As illustrated in Figure 8, the electrochemical stability limitations of sulfide-based SSEs stem from their narrow ESW compared to other electrolyte systems. The instability of SSEs under extreme lithium chemical potentials, coupled with their inherent reactivity with electrode materials, necessitates both surface and bulk modifications. For instance, coatings such as Li_3PO_4 or $LiTi_2(PO_4)_3$ on NCM cathodes effectively suppress decomposition, while bulk doping strategies improve stability without sacrificing ionic conductivity [185–187].



Figure 7. Interface engineering for inhibiting side reactions [72]. (**a**) Schematic diagram and requirements of the cathode surface coating. (**b**) $LinBo_3$-coated NCM811 cathode [178]. Reprinted with permission from Ref. [72]. Copyright 2023, Elsevier.

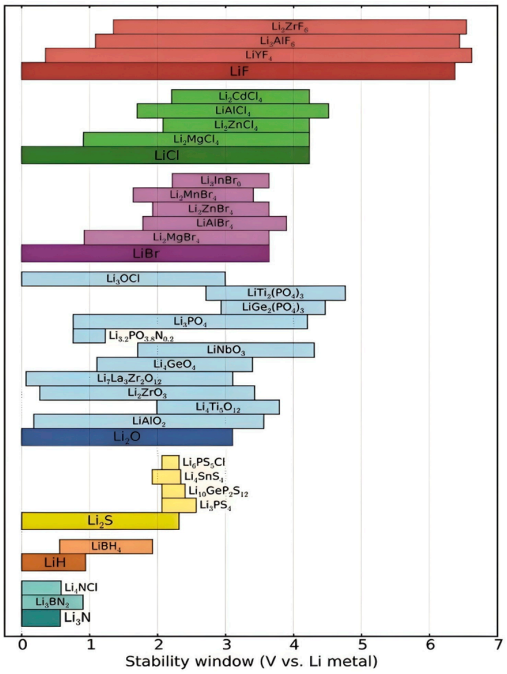


Figure 8. ESW of different electrolyte materials [129]. Reproduced with permission from Ref. [146]. Copyright 2021, Wiley-VCH.

A systematic screening of 41 coating materials identified oxides, such as Li_5TaO_5, as promising candidates for interfacial passivation, as demonstrated in Figure 9 [187].

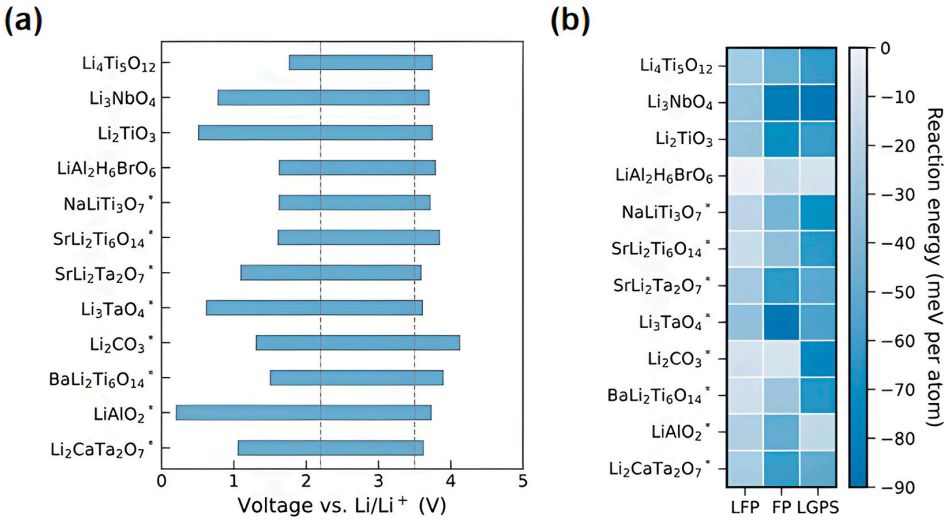


Figure 9. Oxide materials for plating and their electrochemical stability [187]. (**a**,**b**) Reprinted with permission from Ref. [187]. Copyright 2024, Royal Society of Chemistry.

Mechanical instability at solid–solid interfaces stems from the inherent rigidity of sulfide-based SSEs, which are unable to accommodate the significant volume changes associated with silicon anodes (up to 300% expansion) or lithium metal deposition [72]. As shown in Figure 10, contact loss at the anode/SSE interface localizes current density, promoting dendritic Li penetration even in grain-boundary-free glassy electrolytes [178,179]. Strategies to mitigate this include using single-crystal $Li_6La_3ZrTaO_{12}$ garnet electrolytes to eliminate grain boundaries and exerting external pressure (1–10 MPa) to maintain interfacial contact [188–193].

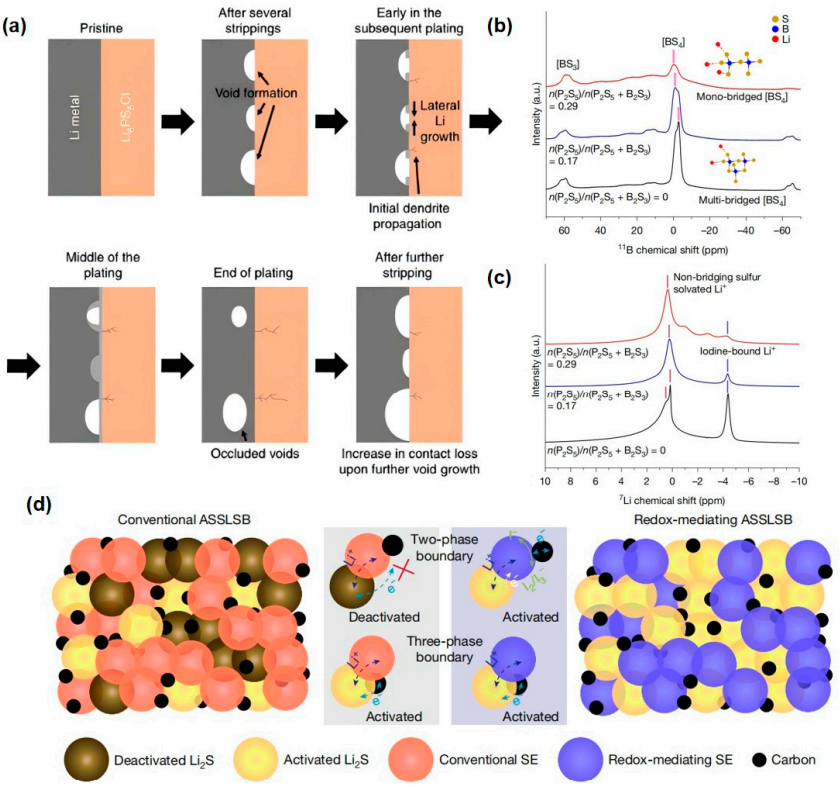


Figure 10. (**a**) Lithium ions penetrate into the SSE layer and form dendrites through defects, resulting in a short circuit [72,191]. (**a**) Reprinted with permission from Ref. [72]. Copyright 2023, Elsevier. (**b**,**c**) Local structural analysis of the three electrolytes using ^{11}B (**b**) and ^{7}Li (**c**) MAS NMR. (**d**) Schematic showing the design principle for the fast-charging mechanism of sulfide-based ASSBs. The redox-mediating SE shown in blue is moderately redox active and generates surficial I_2/I_3 to mediate the sulfur reaction on fast charge [22]. (**b**–**d**) Reprinted with permission from Ref. [22]. Copyright 2025, Springer Nature.

Song et al. synthesized a series of novel glassy sulfide LBPSI (Li_2S-B_2S_3-P_2S_5-LiI) electrolyte materials for application in sulfide-based ASSBs, achieving rapid solid–solid sulfur electrochemistry and high cycling stability. This electrolyte not only serves as an ultra-ionic conductor within the sulfur cathode but also contains redox-active iodine elements that exert a surface redox-mediated role in the solid–solid sulfur conversion process, thereby facilitating the efficient oxidation of Li_2S. This redox-mediated process at the SSE surface enables reactions at the SE | Li_2S dual-phase boundaries, significantly increasing the density of active sites as illustrated in Figure 10a [22].

By adjusting the ratio of B_2S_3 and P_2S_5 glass formers, Song et al. designed a family of LBPSI glass electrolytes with high ionic conductivity ($P_2S_5/(P_2S_5 + B_2S_3)$ mol/mol ratio of 0.80; $n(P_2S_5)/n(P_2S_5 + B_2S_3)$ hereafter). As shown in Figure 10b, ^{11}B solid-state NMR spectra reveal that when the molar ratio of P_2S_5 reaches $n(P_2S_5)/n(P_2S_5 + B_2S_3) = 0.17$, the peak corresponding to $[BS_4]$ structural units shifts toward higher frequencies (from

−2.88 ppm to −1.01 ppm), indicating a transition from multi-bridging to single-bridging configurations in the [BS_4] units [194–196]. This observation demonstrates the fragmentation of the B-S network and the formation of smaller island-like local structures with reduced rigidity, which facilitates Li^+ migration [22].

The ^7Li NMR spectra in Figure 10c show that at $n(P_2S_5)/n(P_2S_5 + B_2S_3) = 0.17$, the peak corresponding to Li^+ associated with iodine (−4.4 ppm) diminishes significantly, suggesting an improved integration of Li^+/I^- ions and a reduction in isolated ion pairs [22]. Furthermore, the shoulder peaks (0.50 and 0.17 ppm) attributed to Li^+ coordinated with non-bridging sulfur evolve into a single peak at 0.22 ppm, reflecting weakened nuclear shielding effects that promote Li^+ mobility [197,198].

In addition to interfacial challenges, air sensitivity poses a significant barrier to the practical application of sulfide-based SSEs [199]. When exposed to humid environments, sulfide SSEs undergo hydrolysis, releasing H_2S and resulting in a decline in ionic conductivity [200]. Notably, the $75Li_2S{\cdot}25P_2S_5$ glass–ceramic demonstrates exceptional air stability, retaining a conductivity of 1.5×10^{-4} S·cm^{-1} even after 7 h of air exposure [79]. Oxygen doping (e.g., LPSO) or hydrophobic coatings like g-C_3N_4 suppress H_2S generation [201]. As demonstrated in Figure 11, g-C_3N_4-coated(651-5%, 651-5%-exposure) LPSC retains 72% conductivity after air exposure, compared to 52% for uncoated samples(651, 651-exposure) [200]. Ni et al. successfully synthesized a $Li_{3.12}P_{0.94}Bi_{0.06}S_{3.91}O_{0.09}$ sulfide solid electrolyte by co-doping Li_3PS_4 with Bi and O, which exhibits enhanced air stability. Air stability tests were conducted by exposing $Li_{3+2x}P_{1-x}Bi_xS_{4-1.5x}O_{1.5x}$ electrolytes with varying doping levels to air under 50% relative humidity [93]. As shown in Figure 10c,d, undoped Li_3PS_4 readily reacts with H_2O, releasing significant amounts of H_2S gas. In contrast, Bi- and O- doped Li_3PS_4 electrolytes demonstrate suppressed reactivity with H_2O, with the release of H_2S gas progressively decreasing as doping levels increase. As shown in Figure 10b, X-ray diffraction (XRD) measurements reveal that the $Li_{3.12}P_{0.94}Bi_{0.06}S_{3.91}O_{0.09}$ electrolyte maintains structural integrity in air, whereas undoped Li_3PS_4 undergoes substantial structural degradation, as evidenced by the emergence of numerous impurity peaks after air exposure [202].

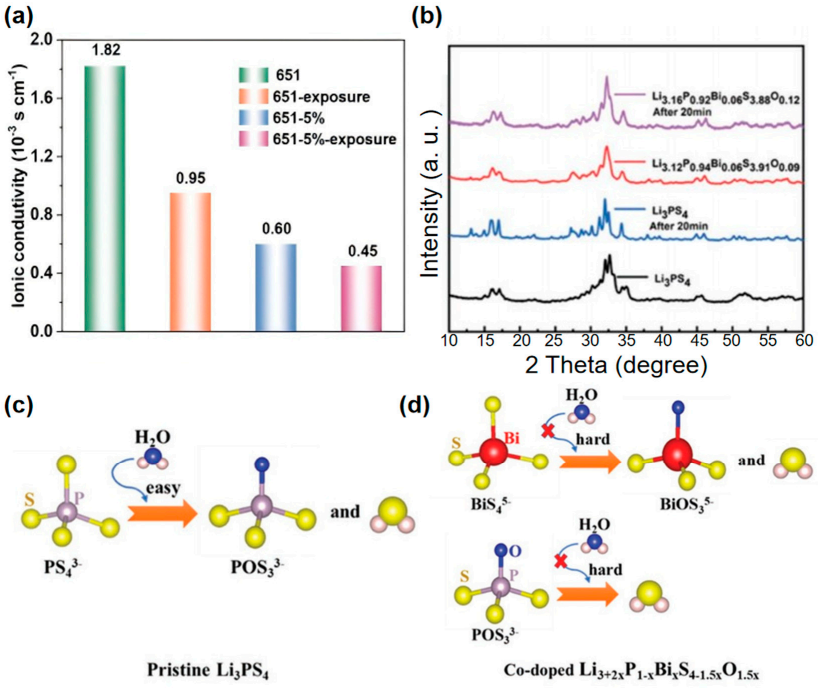


Figure 11. (**a**) Impedance spectra of 651 and 651-5% SSEs before and after exposure to air [203]. Reproduced with permission from Ref. [203]. Copyright 2024, Wiley-VCH. (**b**) The XRD patterns of Li_3PS_4 and $Li_{3.12}P_{0.94}Bi_{0.06}S_{3.91}O_{0.09}$ that were exposed to wet air. (**c**) Chemical stability theory of Li_3PS_4

and (**d**) co-doped $Li_{3.12}P_{0.94}Bi_{0.06}S_{3.91}O_{0.09}$. (**b**–**d**) Reprinted with permission from Ref. [204]. Copyright 2022, Wiley-VCH.

5.2. Conductivity Optimization of Sulfide SSEs

The ionic conductivity of sulfide SSEs is governed by anion disorder and lattice dynamics, which can be strategically engineered through structural modifications and doping strategies [205].

In Li_6PS_5X (X = F, Cl, Br, I) electrolytes, the degree of S^{2-}/X^- mixing directly dictates Li^+ migration pathways. For X = Cl and Br, the similar ionic radii of S^{2-} (1.84 Å), Cl^- (1.81 Å), and Br^- (1.96 Å) promote anion disorder, broadening Li^+ transport channels and achieving more than 1×10^{-2} S·cm^{-1} [206]. In contrast, the large size mismatch between S^{2-} and I^- (2.20 Å) in Li_6PS_5I induces ordered anion arrangements, reducing mixing and resulting in lower conductivity (10^{-5} S·cm^{-1}) [206]. Additionally, softer lattices with enhanced bond flexibility lower Li^+ migration energy barriers, further improving ionic transport [26,207].

Doping with aliovalent cations (e.g., Si^{4+}, Ge^{4+}) or anions (e.g., I^-) enhances both ionic conductivity and electrochemical stability [27]. For instance, Si^{4+} doping in Li_6PS_5Br increases S^{2-}/Br^- disorder, with $Li_{6.35}P_{0.65}Si_{0.35}S_5Br$ reaching 2.4×10^{-3} S·cm^{-1} at 25 °C [86]; Ge^{4+} doping in Li_6PS_5I elevates S^{2-}/I^- mixing, yielding $Li_{6.6}P_{0.4}Ge_{0.6}S_5I$ with $(18.4 \pm 2.7) \times 10^{-3}$ S·cm^{-1} [207]; and MoS_2 doping in $Li_7P_3S_{11}$ produces $Li_7P_{2.9}S_{10.85}Mo_{0.01}$, achieving 4.8 mS·cm^{-1} and a widened ESW (5V vs. Li/Li$^+$) [208].

These modifications not only improve Li^+ mobility, but also enhance compatibility with lithium metal anodes, as demonstrated by Sb-doped β-Li_3PS_4 ($Li_3P_{0.98}Sb_{0.02}S_{3.95}O_{0.05}$, 1.08 mS·cm^{-1}) [209–212].

Quenching protocols play a critical role in modulating ionic conductivity by controlling the degree of anion disorder. As shown in Figure 12a,b, theoretical and experimental studies on Li_6PS_5Br reveal that rapid quenching amplifies S^{2-}/Br^- mixing, increasing Li^+–anion distances and weakening Coulombic interactions. This delocalization effect elevates conductivity from 5×10^{-4} S·cm^{-1} (slow cooling) to 2×10^{-3} S·cm^{-1} (quenching) [211]. Such process-dependent structural tuning highlights the critical role of synthesis kinetics in optimizing sulfide SSE performance.

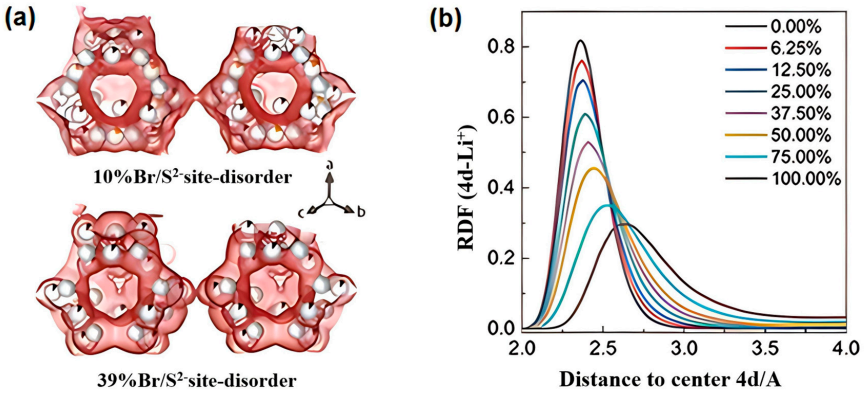


Figure 12. (**a**) The maximum entropy method is used to analyze the migration path of lithium ions [54]. (**b**) The influence of S^{2-}/Br^- disorder on the radial distribution function of lithium ions at the 4d site [211]. (**a**,**b**) Reprinted with permission from Ref. [54]. Copyright 2023, Elsevier.

5.3. Mechanical Stability of Sulfide SSEs

The mechanical stability of sulfide-based SSEs is fundamentally tied to their ionic conductivity and interfacial integrity, which are critical factors determining the cycle life and safety of ASSBs. Despite their superior ionic conductivity, sulfide SSEs encounter

significant challenges for large-scale deployment, primarily due to limited electrochemical stability and mechanical degradation under operational stress conditions [212–214].

During charge–discharge cycles, the volumetric expansion/contraction of active materials (e.g., silicon anodes with 300% volume change) and the inherent rigidity of sulfide SSEs induce interfacial delamination and crack propagation at the electrode–electrolyte interface [72]. Unlike liquid electrolytes, sulfide SSEs cannot dynamically adapt to these volume changes, leading to stress accumulation and the eventual mechanical failure of composite electrodes [215]. Advanced characterization techniques, such as X-ray computed tomography and transmission X-ray microscopy, enable real-time observation of crack formation and contact loss at solid–solid interfaces, while focused ion beam-SEM provides 3D microstructural insights into degradation mechanisms [216,217].

To mitigate these issues, strategies include applying external pressure (1–10 MPa) to maintain interfacial contact and suppress crack initiation; utilizing low-strain active materials (e.g., $Li_4Ti_5O_{12}$) to minimize volume changes; and optimizing the distribution of SSE, conductive additives, and voids within composite electrodes [218–221].

These approaches underscore the need for holistic material design to balance ionic transport and mechanical resilience in sulfide-based ASSBs.

Dealloying, the selective removal of one or more components from an alloy, is widely employed to fabricate metallic materials with tailored nano-porosity and composition. Compared to conventional materials, dealloyed metals exhibit superior porosity and tunable structural characteristics, demonstrating unique advantages in battery technologies and other advanced applications. However, the mechanical stress effects during dealloying processes remain insufficiently explored, particularly in solid-state battery systems. A critical challenge lies in effectively controlling structural evolution and electrochemical performance during alloying/dealloying cycles [222–225].

Wang et al. investigated the influence of stacking pressure on the alloying/dealloying behavior of lithium-alloyable materials (Al and Si). By analyzing porosity evolution during alloying/dealloying processes in both solid-state and liquid electrolytes (Figure 13a,b), they systematically compared silicon wafer electrodes (0.38 V and 1.0 V vs. Li/Li^+) under varying stacking pressures (0.5 MPa, 2 MPa, 10 MPa, and 30 MPa) [73]. Their findings revealed distinct morphological transformations in dealloyed metals across electrolyte types (Figure 13c,d). Stacking pressure emerged as a decisive factor in porosity regulation: At lower pressures (2–5 MPa), indium-coated interfaces significantly enhanced interfacial contact, enabling reversible lithium storage with high areal capacity retention and cycling efficiency. This work provides critical insights into interface engineering for optimizing alloy-based anodes in energy storage systems.

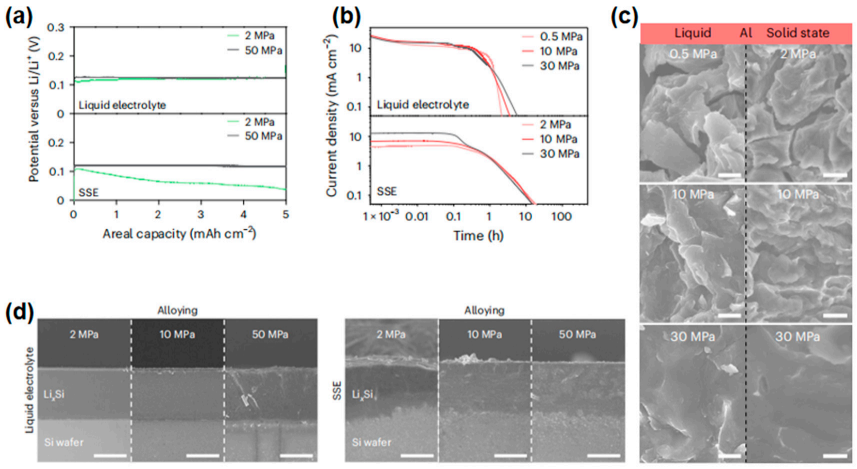


Figure 13. (**a**,**b**) Current density curves of constant potential dealloying tests of liquid electrolyte and SSE under different stacking pressures [218]. (**a**) Under the condition of 0.38 V (relative to Li/Li^+ 1.0 V),

the research object is the Al electrode. (**b**) The current density is 0.1 mA·cm^{-2}, and the research object is a Si sheet electrode. (**c**,**d**) Cross-sectional SEM images of the electrode after electrochemical dealloying under different stacking pressures [218]. (**c**) Al, showing the liquid electrolyte (**left**) and SSE (**right**). (**d**) Cross-sectional SEM images of Si sheet electrodes after electrochemical alloying at 5 mA·h^{-2} using liquid electrolyte (**left**) and SSE (**right**) at different stacking pressures, as shown in the figure (**a**–**d**). Reprinted with permission from Ref. [218]. Copyright 2025, NPG.

5.4. Emerging Research Directions and Opportunities

The development of sulfide-based SSEs for ASSBs necessitates overcoming three key interconnected challenges: understanding ion transport mechanisms, suppressing lithium dendrite formation, and addressing multi-field coupling effects [226–228].

Ion transport mechanisms: Although sulfide-based SSEs demonstrate high bulk ionic conductivity, the atomic-scale dynamics of Li^+ migration—particularly the interaction between lattice phonons and interfacial processes—remain insufficiently understood. Current limitations in real-time characterization techniques, such as operando spectroscopy, and computational models impede the optimization of ion transport pathways. The development of advanced tools, including neutron pair distribution function (PDF) analysis and machine learning-driven molecular dynamics simulations, will be essential for elucidating these mechanisms and guiding the design of improved materials [229–231].

Lithium dendrite growth: despite the mechanical robustness of sulfide SSEs (>1GPa hardness), lithium dendrites propagate through grain boundaries and defects, threatening cell safety [191]. Future studies must resolve the nucleation and growth kinetics of Li metal within SSEs under operational conditions (e.g., current density and pressure). Strategies such as artificial SEI layers and lattice strain engineering could homogenize Li deposition, but their long-term efficacy requires validation through coupled experimental–theoretical approaches [232].

Multi-field coupling effects: ASSBs operate under complex multi-physics coupling conditions, where localized hotspots, stress gradients, and interfacial reactions interact synergistically, leading to accelerated degradation. Establishing predictive multi-physics models that integrate these interactions is essential to decode failure mechanisms (e.g., crack propagation and impedance rise) and optimize cell designs. For instance, phase-field modeling combined with in situ X-ray tomography could map stress distributions during cycling, informing pressure management strategies [233–236].

Ultimately, bridging nanoscale material insights with macroscale battery performance will require interdisciplinary collaboration across materials science, electrochemistry, and computational modeling.

6. Conclusions

6.1. Research Status and Challenges

Sulfide SSEs present a dual challenge: enhancing ionic conductivity to maximize battery performance and improving air stability to enable cost-effective large-scale production. This review systematically examines the fundamental properties of sulfide SSEs, including their chemical composition, ionic conduction mechanisms, and physicochemical characteristics, while evaluating their applicability in ASSBs. Critical issues such as air sensitivity and interfacial side reactions are analyzed, providing a theoretical foundation for designing high-energy-density, long-cycle-life ASSBs [198].

Despite advancements in ionic conductivity, sulfide SSEs face significant barriers to commercialization, including rapid hydrolysis in humid environments and interfacial degradation during cycling. Recent progress in anion doping (e.g., oxygen incorporation)

and surface coating strategies has demonstrated promising results in suppressing H_2S generation and enhancing electrochemical stability [224–238]. However, achieving scalable production requires the further optimization of synthesis protocols to reduce costs below $50/kg while maintaining mechanical and chemical integrity [54,168].

6.2. Future Perspectives

Realizing the full potential of sulfide-based ASSBs requires coordinated advancements across material design, manufacturing processes, characterization techniques, and system integration.

Material innovation requires compositional engineering to develop cost-effective batch production methods for sulfide SSEs and thin-film electrolytes, coupled with advanced doping strategies (e.g., halogen or oxide incorporation) to improve atmospheric stability and interfacial compatibility with high-capacity electrodes such as silicon–carbon anodes [225–237]. Concurrently, manufacturing processes must transition from energy-intensive synthesis to scalable techniques like roll-to-roll processing, ensuring compatibility with high-voltage cathodes (e.g., NCM811) and lithium metal anodes while reducing production costs [90]. Advanced characterization urgently demands in situ/operando methodologies to overcome material air sensitivity, exemplified by differential phase-contrast STEM for solid-concentration layer analysis and coupled in situ NMR/Raman spectroscopy for probing dynamic interfacial evolution during cycling [239]. Cell architecture optimization focuses on reducing SSE membrane thickness below 20 μm to achieve energy densities exceeding 400 Wh/kg, though mechanical robustness challenges necessitate innovative solutions like flexible polymer binders or organic–inorganic hybrid matrices [28,240]. Finally, comprehensive safety protocols must integrate multi-physics modeling frameworks that couple electrochemical, thermal, and mechanical parameters to evaluate extreme-condition behaviors (e.g., thermal runaway and mechanical stress), thereby guiding the design of durable battery systems [214].

6.3. Challenges and Prospects for Commercialization

The commercialization of sulfide-based ASSBs necessitates interdisciplinary efforts to address key challenges in material synthesis, interface engineering, and scalable production. With coordinated policy frameworks and sustained R&D investment, sulfide-based SSEs are expected to overcome existing limitations, paving the way for the widespread adoption of safe, high-energy-density ASSBs within the next decade. Such advancements will significantly contribute to global carbon neutrality goals and the development of sustainable energy storage solutions.

Author Contributions: B.M.: Writing—review and editing, Investigation. Y.Z., Q.L., Y.C., X.L., W.L., Z.Z., C.H. and M.J.: Writing—review and editing. S.L.: Writing—review and editing, Investigation, Resources, Conceptualization. All authors have read and agreed to the published version of the manuscript.

Funding: This research received no external funding.

Data Availability Statement: No data were used for the research described in this article.

Conflicts of Interest: The authors declare no conflicts of interest.

References

1. Dunn, B.; Kamath, H.; Tarascon, J.-M. Electrical Energy Storage for the Grid: A Battery of Choices. *Science* **2011**, *334*, 928–935. [CrossRef]
2. Goodenough, J.B. Electrochemical energy storage in a sustainable modern society. *Energy Environ. Sci.* **2014**, *7*, 14–18. [CrossRef]
3. Janek, J.; Zeier, W.G. A solid future for battery development. *Nat. Energy* **2016**, *1*, 16141. [CrossRef]

4. Kim, K.J.; Balaish, M.; Wadaguchi, M.; Kong, L.; Rupp, J.L.M. Solid-State Li-Metal Batteries: Challenges and Horizons of Oxide and Sulfide Solid Electrolytes and Their Interfaces. *Adv. Energy Mater.* **2020**, *11*, 2002689. [CrossRef]
5. Yang, X.; Luo, J.; Sun, X. Towards high-performance solid-state Li-S batteries: From fundamental understanding to engineering design. *Chem. Soc. Rev.* **2020**, *49*, 2140–2195. [CrossRef]
6. Fan, L.-Z.; He, H.; Nan, C.-W. Tailoring inorganic-polymer composites for the mass production of solid-state batteries. *Nat. Rev. Mater.* **2021**, *6*, 1003–1019. [CrossRef]
7. Xiao, Y.; Turcheniuk, K.; Narla, A.; Song, A.-Y.; Ren, X.; Magasinski, A.; Jain, S.; Huang, S.; Lee, H.; Yushin, G. Electrolyte melt infiltration for scalable manufacturing of inorganic all-solid-state lithium-ion batteries. *Nat. Mater.* **2021**, *20*, 984–990. [CrossRef]
8. Wang, W.; Li, Y.; Cheng, L.; Zuo, F.; Yang, S. Safety performance and failure prediction model of cylindrical lithium-ion battery. *J. Power Sources* **2020**, *451*, 227755. [CrossRef]
9. Lau, J.; DeBlock, R.H.; Butts, D.M.; Ashby, D.S.; Choi, C.S.; Dunn, B.S. Sulfide Solid Electrolytes for Lithium Battery Applications. *Adv. Energy Mater.* **2018**, *8*, 1800933. [CrossRef]
10. Park, K.H.; Bai, Q.; Kim, D.H.; Oh, D.Y.; Zhu, Y.; Mo, Y.; Jung, Y.S. Design Strategies, Practical Considerations, and New Solution Processes of Sulfide Solid Electrolytes for All-Solid-State Batteries. *Adv. Energy Mater.* **2018**, *8*, 1800035. [CrossRef]
11. Chen, S.; Xie, D.; Liu, G.; Mwizerwa, J.P.; Zhang, Q.; Zhao, Y.; Xu, X.; Yao, X. Sulfide solid electrolytes for all-solid-state lithium batteries: Structure, conductivity, stability and application. *Energy Storage Mater.* **2018**, *14*, 58–74. [CrossRef]
12. Kamaya, N.; Homma, K.; Yamakawa, Y.; Hirayama, M.; Kanno, R.; Yonemura, M.; Kamiyama, T.; Kato, Y.; Hama, S.; Kawamoto, K.; et al. lithium superionic conductor. *Nat. Mater.* **2011**, *10*, 682–686. [CrossRef]
13. Bron, P.; Johansson, S.; Zick, K.; Schmedt auf der Günne, J.; Dehnen, S.; Roling, B. $Li_{10}SnP_2S_{12}$: An Affordable Lithium Superionic Conductor. *J. Am. Chem. Soc.* **2013**, *135*, 15694–15697. [CrossRef] [PubMed]
14. Lewis, J.A.; Cortes, F.J.Q.; Liu, Y.; Miers, J.C.; Verma, A.; Vishnugopi, B.S.; Tippens, J.; Prakash, D.; Marchese, T.S.; Han, S.Y.; et al. Linking void and interphase evolution to electrochemistry in solid-state batteries using operando X-ray tomography. *Nat. Mater.* **2021**, *20*, 503–510. [CrossRef]
15. Tan, D.H.S.; Wu, E.A.; Nguyen, H.; Chen, Z.; Marple, M.A.T.; Doux, J.-M.; Wang, X.; Yang, H.; Banerjee, A.; Meng, Y.S. Elucidating Reversible Electrochemical Redox of Li_6PS_5Cl Solid Electrolyte. *ACS Energy Lett.* **2019**, *4*, 2418–2427. [CrossRef]
16. Wang, S.; Tang, M.; Zhang, Q.; Li, B.; Ohno, S.; Walther, F.; Pan, R.; Xu, X.; Xin, C.; Zhang, W.; et al. Lithium Argyrodite as Solid Electrolyte and Cathode Precursor for Solid-State Batteries with Long Cycle Life. *Adv. Energy Mater.* **2021**, *11*, 2101370. [CrossRef]
17. Yu, C.; Zhao, F.; Luo, J.; Zhang, L.; Sun, X. Recent development of lithium argyrodite solid-state electrolytes for solid-state batteries: Synthesis, structure, stability and dynamics. *Nano Energy* **2021**, *83*, 105858. [CrossRef]
18. Quintero, M.A.; Hao, S.; Patel, S.V.; Bao, J.-K.; Zhou, X.; Hu, Y.-Y.; Wolverton, C.; Kanatzidis, M.G. Lithium Thiostannate Spinels: Air-Stable Cubic Semiconductors. *Chem. Mater.* **2021**, *33*, 2080–2089. [CrossRef]
19. Wang, S.; Zhang, X.; Liu, S.; Xin, G.; Xue, C.; Richter, F.; Li, L.; Fan, L.; Lin, Y.; Shen, Y. High-conductivity free-standing Li_6PS_5Cl/poly(vinylidene difluoride) composite solid electrolyte membranes for lithium-ion batteries. *ACS Appl. Mater. Interfaces* **2020**, *6*, 70–76. [CrossRef]
20. Zhang, S.M.; Zhao, F.P.; Su, H.; Zhong, Y.; Liang, J.W.; Chen, J.T.; Zheng, M.L.; Liu, J.; Chang, L.Y.; Fu, J.M.; et al. Cubic Iodide Li_xYI_{3+x} Superionic Conductors through Defect Manipulation for All-Solid-State Li Batteries. *Angew. Chem. Int. Ed.* **2024**, *63*, e202316360. [CrossRef]
21. Jin, H.; Lei, J.; Hussain, F.; Tang, W.; Zhao, C.; Yu, P.; Li, Y.; Liu, M.; Zhang, J.; Yin, W.; et al. Regulating Chemical Bonds in Halide Frameworks for Lithium Superionic Conductors. *ACS Nano* **2025**, *19*, 6399–6411. [CrossRef] [PubMed]
22. Song, H.; Münch, K.; Liu, X.; Shen, K.; Zhang, R.; Weintraut, T.; Yusim, Y.; Jiang, D.; Hong, X.; Meng, J.; et al. All-solid-state Li-S batteries with fast solid-solid sulfur reaction. *Nature* **2025**, *637*, 846–853. [CrossRef]
23. Kato, Y.; Hori, S.; Saito, T.; Suzuki, K.; Hirayama, M.; Mitsui, A.; Yonemura, M.; Iba, H.; Kanno, R. High-power all-solid-state batteries using sulfide superionic conductors. *Nat. Energy* **2016**, *1*, 16030. [CrossRef]
24. Deiseroth, H.-J.; Kong, S.-T.; Eckert, H.; Vannahme, J.; Reiner, C.; Zaiß, T.; Schlosser, M. Li_6PS_5X: A Class of Crystalline Li-Rich Solids With an Unusually High Li^+ Mobility. *Angew. Chem. Int. Ed.* **2008**, *47*, 755–758. [CrossRef]
25. Seino, Y.; Ota, T.; Takada, K.; Hayashi, A.; Tatsumisago, M. A sulphide lithium super ion conductor is superior to liquid ion conductors for use in rechargeable batteries. *Energy Environ. Sci.* **2014**, *10*, 1039. [CrossRef]
26. Zhou, L.; Assoud, A.; Zhang, Q.; Wu, X.; Nazar, L.F. New Family of Argyrodite Thioantimonate Lithium Superionic Conductors. *J. Am. Chem. Soc.* **2019**, *141*, 19002–19013. [CrossRef] [PubMed]
27. Rangasamy, E.; Liu, Z.; Gobet, M.; Pilar, K.; Sahu, G.; Zhou, W.; Wu, H.; Greenbaum, S.; Liang, C. An Iodide-Based $Li_7P_2S_8I$ Superionic Conductor. *J. Am. Chem. Soc.* **2015**, *137*, 1384–1387. [CrossRef]
28. Li, Y.; Song, S.; Kim, H.; Nomoto, K.; Kim, H.; Sun, X.; Hori, S.; Suzuki, K.; Matsui, N.; Hirayama, M.; et al. A lithium superionic conductor for millimeter-thick battery electrode. *Science* **2023**, *381*, 50–53. [CrossRef]
29. Boulineau, S.; Courty, M.; Tarascon, J.-M.; Viallet, V. Mechanochemical synthesis of Li-argyrodite Li_6PS_5X(X=Cl,Br,I) as sulfur-based solid electrolytes for all solid state batteries application. *Solid State Ion.* **2012**, *221*, 1–5. [CrossRef]

30. Adeli, P.; Bazak, J.D.; Park, K.H.; Kochetkov, I.; Huq, A.; Goward, G.R.; Nazar, L.F. Boosting Solid-State Diffusivity and Conductivity in Lithium Superionic Argyrodites by Halide Substitution. *Angew. Chem. Int. Ed.* **2019**, *58*, 8681–8686. [CrossRef]
31. Lee, Y.; Jeong, J.; Lee, H.J.; Kim, M.; Han, D.; Kim, H.; Yuk, J.M.; Nam, K.-W.; Chung, K.Y.; Jung, H.-G.; et al. Lithium argyrodite sulfide electrolytes with high ionic conductivity andair stability for all-solid-state Li-ion batteries. *ACS Energy Lett.* **2022**, *7*, 171–179. [CrossRef]
32. Wang, Y.; Qu, H.; Liu, B.; Li, X.; Ju, J.; Li, J.; Zhang, S.; Ma, J.; Li, C.; Hu, Z.; et al. Self-organized hetero-nanodomains actuating super Li^+ conduction in glass ceramics. *Nat. Commun.* **2023**, *14*, 669. [CrossRef]
33. Su, H.; Zhong, Y.; Wang, C.; Liu, Y.; Hu, Y.; Li, J.; Wang, M.; Jiao, L.; Zhou, N.; Xiao, B.; et al. Deciphering the critical role of interstitial volume in glassy sulfide superionic conductors. *Nat. Commun.* **2024**, *15*, 2552. [CrossRef] [PubMed]
34. Ming, L.; Deng, M.; Li, S.W.; Jiang, Z.L.; Li, L.; Lu, Z.Y.; Luo, Q.Y.; Yang, J.; Cui, Z.H.; Yu, C. Reviving the ionic conductivity of air-instable solid-state electrolytes via a facile heat treatment. *Chin. Chem. Lett.* **2025**, *111114*, 1001–8417. [CrossRef]
35. Liu, J.; Yuan, H.; Liu, H.; Zhao, C.-Z.; Lu, Y.; Cheng, X.-B.; Hang, J.-Q.; Zhang, Q. Unlocking the Failure Mechanism of Solid State Lithium Metal Batteries. *Sus Mat.* **2021**, *1*, 38–50. [CrossRef]
36. Manthiram, A.; Yu, X.; Wang, S. Lithium battery chemistries enabled by solid-state electrolytes. *Nat. Rev. Mater.* **2017**, *2*, 16103. [CrossRef]
37. Wang, L.; Yi, S.; Liu, Q.; Li, Y.; Hu, Y.; Tu, H.; Wang, Y.; Sun, A.; Zhu, F.; Mushtaq, F.; et al. Bifunctional lithium-montmorillonite enabling solid electrolyte with superhigh ionic conductivity for high-performanced lithium metal batteries. *Energy Storage Mater.* **2023**, *63*, 102961. [CrossRef]
38. Fan, X.; Wang, C. High-voltage liquid electrolytes for Li batteries: Progress and perspectives. *Chem. Soc. Rev.* **2021**, *50*, 10486–10566. [CrossRef]
39. Zhang, W.; Seo, D.-H.; Chen, T.; Wu, L.; Topsakal, M.; Zhu, Y.; Lu, D.; Ceder, G.; Wang, F. Kinetic pathways of ionic transport in fast-charging lithium titanate. *Science* **2020**, *367*, 1030–1034. [CrossRef]
40. Cheng, Y.; Shu, J.; Xu, L.; Xia, Y.; Du, L.; Zhang, G.; Mai, L. Flexible Nanowire Cathode Membrane with Gradient Interfaces and Rapid Electron/Ion Transport Channels for Solid-State Lithium Batteries. *Adv. Energy Mater.* **2021**, *11*, 2100026. [CrossRef]
41. Zhao, Q.; Stalin, S.; Zhao, C.-Z.; Archer, L.A. Designing solid-state electrolytes for safe, energy-dense batteries. *Nat. Rev. Mater.* **2020**, *5*, 229–252. [CrossRef]
42. Zuo, D.; Yang, L.; Zou, Z.; Li, S.; Feng, Y.; Harris, S.J.; Shi, S.; Wan, J. Ultrafast Synthesis of NASICON Solid Electrolytes for Sodium-Metal Batteries. *Adv. Energy Mater.* **2023**, *13*, 2301540. [CrossRef]
43. Ferrer-Nicomedes, S.; Mormeneo-Segarra, A.; Vicente-Agut, N.; Barba-Juan, A. Introducing an ionic conductive matrix to the cold-sintered $Li_{1.3}Al_{0.3}Ti_{1.7}(PO_4)^{3-}$ based composite solid electrolyte to enhance the electrical properties. *J. Power Sources* **2023**, *581*, 233494. [CrossRef]
44. Anderson, E.; Zolfaghar, E.; Jonderian, A.; Khaliullin, R.Z.; McCalla, E. Comprehensive Dopant Screening in $Li_7La_3Zr_2O_{12}$ Garnet Solid Electrolyte. *Adv. Energy Mater.* **2024**, *14*, 2304025. [CrossRef]
45. Xu, S.; Zhang, K.; Xu, R.; Tang, P.; Cheng, H.-M.; Sun, Z.; Li, F. Adaptive ion diffusion in a highly crystalline pure polymer for stable solid-state batteries. *Energy Storage Mater.* **2025**, *74*, 103941. [CrossRef]
46. Dai, C.; Weng, M.; Cai, B.; Liu, J.; Guo, S.; Xu, H.; Yao, L.; Stadler, F.J.; Li, Z.-M.; Huang, Y.-F. Ion-Conductive Crystals of Poly (vinylidene fluoride) Enables Fast Charging Solid-State Lithium Metal Batteries. *Energy Environ. Sci.* **2024**, *17*, 8243–8253. [CrossRef]
47. Tufail, M.K.; Ahmad, N.; Yang, L.; Zhou, L.; Naseer, M.A.; Chen, R.; Yang, W. A panoramic view of $Li_7P_3S_{11}$ solid electrolytes synthesis, structural aspects and practical challenges for all-solid-state lithium batteries. *Chin. J. Chem. Eng.* **2021**, *39*, 16–36. [CrossRef]
48. Zheng, Q.; Song, Y.; Huang, W.; Yang, J.; Li, T.; Xu, Y. Challenges and strategies towards the interface between lithium anode and $Li_{10}GeP_2S_{12}$ electrolyte in all-solid-state lithium metal batteries. *Energy Storage Mater.* **2023**, *63*, 103038. [CrossRef]
49. Bonsu, J.O.; Bhadra, A.; Kundu, D. Wet Chemistry Route to Li_3InCl_6: Microstructural Control Render High Ionic Conductivity and Enhanced All-Solid-State Battery Performance. *Adv. Sci.* **2024**, *11*, 2403208. [CrossRef]
50. Geng, J.; Yan, Z.; Zhu, Y. Elucidating Anisotropic Ionic Diffusion Mechanism in Li_3YCl_6 with Molecular Dynamics Simulations. *ACS Appl. Energy Mater.* **2024**, *7*, 7019–7024. [CrossRef]
51. Liang, J.; van der Maas, E.; Luo, J.; Li, X.; Chen, N.; Adair, K.R.; Li, W.; Li, J.; Hu, Y.; Liu, J.; et al. A Series of Ternary Metal Chloride Superionic Conductors for High-Performance All-Solid-State Lithium Batteries. *Adv. Energy Mater.* **2022**, *12*, 2103921. [CrossRef]
52. Lennartz, P.; Paren, B.A.; Herzog-Arbeitman, A.; Chen, X.C.; Johnson, J.A.; Winter, M.; Shao-Horn, Y.; Brunklaus, G. Practical considerations for enabling Li | polymer electrolyte batteries. G. *Joule* **2023**, *7*, 1471–1495. [CrossRef]
53. Kang, J.; Yan, Z.; Gao, L.; Zhang, Y.; Liu, W.; Yang, Q.; Zhao, Y.; Deng, N.; Cheng, B.; Kang, W. Improved ionic conductivity and enhancedinterfacial stability of solid polymer electrolytes with porous ferroelectric ceramic nanofibers. *Energy Storage Mater.* **2022**, *53*, 192–203. [CrossRef]

54. Liu, Y.; Yu, T.; Guo, S.; Zhou, H. Designing High-Performance Sulfide-Based All-Solid-State Lithium Batteries: From Laboratory to Practical Application. *Acta Phys.-Chim. Sin.* **2023**, *39*, 2301027. [CrossRef]
55. Wang, S.; Fang, R.; Li, Y.; Liu, Y.; Xin, C.; Richter, F.H.; Nan, C.-W. Interfacial challenges for all-solid-state batteries based on sulfide solid electrolytes. *J. Mater.* **2021**, *7*, 209–218. [CrossRef]
56. Liang, J.; Chen, D.; Adair, K.; Sun, Q.; Holmes, N.G.; Zhao, Y.; Sun, Y.; Luo, J.; Li, R.; Zhang, L.; et al. Insight into Prolonged Cycling Life of 4 V All-Solid-State Polymer Batteries by a High-Voltage Stable Binder. *Adv. Energy Mater.* **2021**, *11*, 2002455. [CrossRef]
57. Jones, G.R.; Whitfield, R.; Wang, H.S.; Watuthanthrige, A.N.D.; Antonopoulou, M.-N.; Lohmann, V.; Anastasaki, A. Harnessing Non-Thermal External Stimuli for Polymer Recycling. *Macromolecules* **2025**, *58*, 2210–2223. [CrossRef] [PubMed]
58. Lv, L.; Zhou, L.; Tufail, M.K.; Yang, L.; Chen, R.; Yang, W. Advances in air stability of sulfide solid electrolytes with high ion conductivity. *Sci. Sin. Chim.* **2020**, *50*, 1031–1044.
59. Chen, S.J.; Nie, L.; Hu, X.; Zhang, Y.; Zhang, Y.; Yu, Y.; Liu, W. Ultrafast Sintering for Ceramic-Based All-Solid-State Lithium-Metal Batteries. *Adv. Mater.* **2022**, *34*, 2200430. [CrossRef]
60. Mills, A.; Yang, G.; Tsai, W.Y.; Chen, X.C.; Sacci, R.L.; Armstrong, B.L.; Hallinan Jr, D.T.; Nanda, J. Adverse Effects of Trace Non-polar Binder on Ion Transport in Free-standing Sulfide Solid Electrolyte Separators. *J. Electrochem. Soc.* **2023**, *170*, 080513. [CrossRef]
61. Ahmad, N.; Sun, S.; Yu, P.; Yang, W. Design Unique Air-Stable and Li–Metal Compatible Sulfide Electrolyte via Exploration of Anion Functional Units for All-Solid-State Lithium–Metal Batteries. *Adv. Funct. Mater.* **2022**, *32*, 2201528. [CrossRef]
62. Hayashi, A.; Komiya, R.; Tatsumisago, M.; Minami, T. Characterization of Li_2S-SiS_2-Li_3MO_3 (M=B, Al, Ga and In) oxysulfide glasses and their application to solid state lithium secondary batteries. *Solid State Ion.* **2002**, *152–153*, 285–290. [CrossRef]
63. Yamauchi, A.; Sakuda, A.; Hayashi, A.; Tatsumisago, M. Preparation and ionic conductivities of (100-x)(0.75Li_2S·0.25P_2S_5)·x$LiBH_4$ glass electrolytes. *J. Power Sources* **2013**, *244*, 707–710. [CrossRef]
64. Zhang, Y.; Chen, K.; Shen, Y.; Lin, Y.; Nan, C.-W. Synergistic effect of processing and composition x on conductivity of xLi_2S-(100-x)P_2S_5 electrolytes. *Solid State Ion.* **2017**, *305*, 1–6. [CrossRef]
65. Wenzel, S.; Weber, D.A.; Leichtweiss, T.; Busche, M.R.; Sann, J.; Janek, J. Interphase formation and degradation of charge transfer kinetics between a lithium metal anode and highly crystalline $Li_7P_3S_{11}$ solid electrolyte. *Solid State Ion.* **2016**, *286*, 24–33. [CrossRef]
66. Wenzel, S.; Randau, S.; Leichtweiß, T.; Weber, D.A.; Sann, J.; Zeier, W.G.; Janek, J. Direct Observation of the Interfacial Instability of the Fast Ionic Conductor $Li_{10}GeP_2S_{12}$ at the Lithium Metal Anode. *Chem. Mater.* **2016**, *28*, 2400–2407. [CrossRef]
67. Schlem, R.; Burmeister, C.F.; Michalowski, P.; Ohno, S.; Dewald, G.F.; Kwade, A.; Zeier, W.G. Energy Storage Materials for Solid-State Batteries: Design by Mechanochemistry. *Adv. Energy Mater.* **2021**, *11*, 2101022. [CrossRef]
68. Balaish, M.; Gonzalez-Rosillo, J.C.; Kim, K.J.; Zhu, Y.; Hood, Z.D.; Rupp, J.L.M. Processing thin but robust electrolytes for solid-state batteries. *Nat. Energy* **2021**, *6*, 227–239. [CrossRef]
69. Xu, J.; Liu, L.; Yao, N.; Wu, F.; Li, H.; Chen, L. Liquid-involved synthesis and processing of sulfide-based solid electrolytes, electrodes, and all-solid-state batteries. *Mater. Today Nano* **2019**, *8*, 100048. [CrossRef]
70. Wang, J.; Hao, J.; Duan, C.; Wang, X.; Wang, K.; Ma, C. A Fluoride-Ion-Conducting Solid Electrolyte with Both High Conductivity and Excellent Electrochemical Stability. *Small* **2022**, *18*, 2104508. [CrossRef]
71. Peng, J.; Wu, D.; Jiang, Z.; Lu, P.; Wang, Z.; Ma, T.; Yang, M.; Li, H.; Chen, L.; Wu, F. Stable Interface between Sulfide Solid Electrolyte and Room-Temperature Liquid Lithium Anode. *ACS Nano* **2023**, *17*, 12706–12722. [CrossRef] [PubMed]
72. Ren, D.; Lu, L.; Hua, R.; Zhu, G.; Liu, X.; Mao, Y.; Rui, X.; Wang, S.; Zhao, B.; Cui, H.; et al. Challenges and opportunities of practical sulfide-based all-solid-state batteries. *Etransportation.* **2023**, *18*, 100272. [CrossRef]
73. Hwang, S.-H.; Seo, S.-D.; Kim, D.-W. A Novel Time-Saving Synthesis Approach for Li-Argyrodite Superionic Conductor. *Adv. Sci.* **2023**, *10*, 2301707. [CrossRef] [PubMed]
74. Lee, J.E.; Park, K.-H.; Kim, J.C.; Wi, T.-U.; Ha, A.R.; Song, Y.B.; Oh, D.Y.; Woo, J.; Kweon, S.H.; Yeom, S.J.; et al. Universal Solution Synthesis of Sulfide Solid Electrolytes Using Alkahest for All-Solid-State Batteries. *Adv. Mater.* **2022**, *34*, 2200083. [CrossRef] [PubMed]
75. Park, B.K.; Kim, H.; Kim, K.S.; Kim, H.S.; Han, S.H.; Yu, J.S.; Hah, H.J.; Moon, J.; Cho, W.; Kim, K.J. Interface Design Considering Intrinsic Properties of Dielectric Materials to Minimize Space-Charge Layer Effect between Oxide Cathode and Sulfide Solid Electrolyte in All-Solid-State Batteries. *Adv. Energy Mater.* **2022**, *12*, 2201208. [CrossRef]
76. Kim, N.Y.; Kim, I.; Bornamehr, B.; Presser, V.; Ueda, H.; Lee, H.J.; Cheong, J.Y.; Jung, J.W. Recent Advances in Nanoengineering of Electrode-Electrolyte Interfaces to Realize High-Performance Li-Ion Batteries. *Energy Environ. Mater.* **2024**, *7*, e12622. [CrossRef]
77. Chen, X.; Mu, Y.; Liao, Z.; Chu, Y.; Kang, S.; Wu, B.; Liao, R.; Han, M.; Li, Y.; Zeng, L. Advancing high-performance one-dimensional Si/carbon anodes: Current status and challenges. *Carbon Neutralization* **2024**, *3*, 199–221. [CrossRef]
78. Hatzell, K.B.; Chen, X.C.; Cobb, C.L.; Dasgupta, N.P.; Dixit, M.B.; Marbella, L.E.; McDowell, M.T.; Mukherjee, P.P.; Verma, A.; Viswanathan, V.; et al. Challenges in Lithium Metal Anodes for Solid-State Batteries. *ACS Energy Lett.* **2020**, *5*, 922–934. [CrossRef]

79. Lu, P.; Wu, D.; Chen, L.; Li, H.; Wu, F. Air Stability of Solid-State Sulfide Batteries and Electrolytes. *Electrochem. Energy Rev.* **2022**, *5*, 3. [CrossRef]
80. Chen, Y.T.; Duquesnoy, M.; Tan, D.H.S.; Doux, J.M.; Yang, H.; Deysher, G.; Ridley, P.; Franco, A.A.; Meng, Y.S.; Chen, Z. Fabrication of High-Quality Thin Solid-State Electrolyte Films Assisted by Machine Learning. *ACS Energ Lett.* **2021**, *6*, 1639–1648. [CrossRef]
81. Wang, Y.; Ju, J.; Dong, S.; Yan, Y.; Jiang, F.; Cui, L.; Wang, Q.; Han, X.; Cui, G. Facile Design of Sulfide-Based all Solid-State Lithium Metal Battery: In Situ Polymerization within Self-Supported Porous Argyrodite Skeleton. *Adv. Funct. Mater.* **2021**, *31*, 2101523. [CrossRef]
82. Zhu, G.L.; Zhao, C.Z.; Peng, H.J.; Yuan, H.; Hu, J.K.; Nan, H.X.; Lu, Y.; Liu, X.Y.; Huang, J.Q.; He, C.X.; et al. A Self-Limited Free-Standing Sulfide Electrolyte Thin Film for All-Solid-State Lithium Metal Batteries. *Adv. Funct. Mater.* **2021**, *31*, 2101985. [CrossRef]
83. Ren, Y.; Cui, Z.; Bhargav, A.; He, J.; Manthiram, A. A Self-Healable Sulfide/Polymer Composite Electrolyte for Long-Life, Low-Lithium-Excess Lithium-Metal Batteries. *Adv. Funct. Mater.* **2021**, *32*, 2106680. [CrossRef]
84. Park, S.H.; Ayyaswamy, A.; Gjerde, J.; Andrews, W.B.; Vishnugopi, B.S.; Drakopoulos, M.; Vo, N.T.; Zhong, Z.; Thornton, K.; Mukherjee, P.P.; et al. Filament-Induced Failure in Lithium-Reservoir-Free Solid-State Batteries. *ACS Energy Lett.* **2025**, *10*, 1174–1182. [CrossRef]
85. Jiang, T.; He, P.; Liang, Y.; Fan, L.-Z. All-dry synthesis of self-supporting thin $Li_{10}GeP_2S_{12}$ membrane and interface engineering for solid state lithium metal batteries. *Chem. Eng. J.* **2021**, *421*, 129965. [CrossRef]
86. Minafra, N.; Culver, S.P.; Krauskopf, T.; Senyshyn, A.; Zeier, W.G. Effect of Si substitution on the structural and transport properties of superionic Li-argyrodites. *J. Mater. Chem. A* **2018**, *6*, 645–651. [CrossRef]
87. Ye, L.; Li, X. A dynamic stability design strategy for lithium metal solid state batteries. *Nat. Vol.* **2021**, *593*, 218–222. [CrossRef]
88. Kim, J.; Eom, M.; Noh, S.; Shin, D. Performance optimization of all-solid-state lithium ion batteries using a Li_2S-P_2S_5 solid electrolyte and $LiCoO_2$ cathode. *Electron. Mater. Lett.* **2012**, *8*, 209–213. [CrossRef]
89. Janek, J.; Zeier, W.G. Challenges in speeding up solid-state battery development. *Nat. Rev. Mater.* **2025**, *10*, 1038. [CrossRef]
90. Liu, S.; Zhou, L.; Han, J.; Wen, K.; Guan, S.; Xue, C.; Zhang, Z.; Xu, B.; Lin, Y.; Shen, Y.; et al. Super Long-Cycling All-Solid-State Battery with Thin Li_6PS_5Cl-Based Electrolyte. *Adv. Energy Mater.* **2022**, *12*, 2200660. [CrossRef]
91. Ye, Q.; Li, X.; Zhang, W.; Xia, Y.; He, X.; Huang, H.; Gan, Y.; Xia, X.; Zhang, J. Slurry-Coated $LiNi_{0.8}Co_{0.1}Mn_{0.1}O_2$–$Li_3InCl_6$ Composite Cathode with Enhanced Interfacial Stability for Sulfide-Based All-Solid-State Batteries. *ACS Appl. Mater. Interfaces* **2023**, *15*, 18878–18888. [CrossRef]
92. Xiao, Y.; Miara, L.J.; Wang, Y.; Ceder, G. Computational screening of cathode coatings for solid-state batteries. *Joule* **2019**, *3*, 1252–1275. [CrossRef]
93. Wang, Y.; Richards, W.D.; Ong, S.P.; Miara, L.J.; Kim, J.C.; Mo, Y.; Ceder, G. Design Principles for Solid-State Lithium Superionic Conductors. *Nat. Mater.* **2015**, *14*, 1026–1031. [CrossRef]
94. Liu, S.; Zhou, L.; Zhong, T.; Wu, X.; Neyts, K. Sulfide/Polymer Composite Solid-State Electrolytes for All-Solid-State Lithium Batteries. *Adv. Energy Mater.* **2024**, *14*, 2403602. [CrossRef]
95. Yuan, H.; Tian, C.; Song, M.; Lin, W.; Huang, T.; Yu, A. Regulating and understanding the compatibility of sulfide composite solid-state electrolyte in nickel-rich lithium metal batteries. *J. Power Sources* **2024**, *602*, 234366. [CrossRef]
96. Tatsumisago, M.; Hama, S.; Hayashi, A.; Morimoto, H.; Minami, T. New Lithium Ion Conducting Glass-Ceramics Prepared from Mechanochemical Li_2S–P_2S_5 Glasses. *Solid State Ion.* **2002**, *154*, 635–640. [CrossRef]
97. Goodenough, J.B.; Pank, K.S. The Li-Ion Rechargeable Battery: A Perspective. *J. Am. Chem. Soc.* **2013**, *135*, 1167–1176. [CrossRef]
98. Mizuno, F.; Hayashi, A.; Tadanaga, K.; Tatsumisago, M. High lithium ion conducting glass-ceramics in the system Li_2S-P_2S_5. *Solid State Ion.* **2006**, *177*, 2721–2725. [CrossRef]
99. Liu, H.; Cheng, X.; Huang, J.; Yuan, H.; Lu, Y.; Yan, C.; Zhu, G.; Xu, R.; Zhao, C.; Hou, L.; et al. Controlling Dendrite Growth in Solid-State Electrolytes. *ACS Energy Lett.* **2020**, *5*, 833–8433. [CrossRef]
100. Wang, C.; Chen, Q. Elucidating the Kinetic Root of the Evolution of the Oriented Nanoporous Metal from Reduction-Induced Decomposition. *Chem. Mater.* **2021**, *33*, 2604–2610. [CrossRef]
101. Nagao, M.; Hayashi, A.; Tatsumisago, M.; Kanetsuku, T.; Tsuda, T.; Kuwabata, S. In situ SEM study of a lithium deposition and dissolution mechanism in a bulk-type solid-state cell with a Li_2S-P_2S_5 solid electrolyte. *Phys. Chem. Chem. Phys.* **2013**, *15*, 18600–18606. [CrossRef] [PubMed]
102. Lee, Y.-G.; Fujiki, S.; Jung, C.; Suzuki, N.; Yashiro, N.; Omoda, R.; Ko, D.-S.; Shiratsuchi, T.; Sugimoto, T.; Ryu, S.; et al. High-energy long-cycling all-solid-state lithium metal batteries enabled by silver-carbon composite anodes. *Nat. Energy* **2020**, *5*, 299–308. [CrossRef]
103. Grill, J.; Popovic-Neuber, J. Cation Conducting Binders: From Liquid to Solid-State Batteries. *ACS Energy Lett.* **2024**, *9*, 4465–4474. [CrossRef]
104. Jung, S.-K.; Gwon, H.; Yoon, G.; Miara, L.J.; Lacivita, V.; Kim, J.-S. Pliable Lithium Superionic Conductor for All-Solid-State Batteries. *ACS Energy Lett.* **2021**, *6*, 2006–2015. [CrossRef]

105. Huo, H.; Janek, J. Silicon as Emerging Anode in Solid-State Batteries. *ACS Energy Lett.* **2022**, *7*, 4005–4016. [CrossRef]
106. Panchal, A.A.; Pennebaker, T.N.T.; Sebti, E.; Li, Y.; Li, Y.; Clément, R.J.; Canepa, P. Compatibility of Halide Bilayer Separators for All-Solid-State Batteries. *ACS Energy Lett.* **2024**, *9*, 5935–5944. [CrossRef]
107. Li, D.; Liu, H.; Wang, C.; Yan, C.; Zhang, Q.; Nan, C.-W.; Fan, L.-Z. High Ionic Conductive, Mechanical Robust Sulfide Solid Electrolyte Films and Interface Design for All-Solid-State Lithium Metal Batteries. *Adv. Funct. Mater.* **2024**, *34*, 2315555. [CrossRef]
108. Zhu, Y.-P.; Chen, X.; Liu, X.-R.; Liu, Y.; Liu, P.; Zha, H.; Qu, G.; Hong, C.; Li, J.; Jiang, Z. Observation of plaid-like spin splitting in a noncoplanar antiferromagnet. *Nature* **2024**, *626*, 523–528. [CrossRef]
109. Cao, D.; Sun, X.; Li, Y.; Anderson, A.; Lu, W.; Zhu, H. Long-Cycling Sulfide-Based All-Solid-State Batteries Enabled by Electrochemo-Mechanically Stable Electrodes. *Adv. Mater.* **2022**, *34*, 2200401. [CrossRef]
110. Shi, J.; Ma, Z.H.; Han, K.; Wan, Q.; Wu, D.; Qu, X.; Li, P. Coupling novel Li_7TaO_6 surface buffering with bulk Ta-doping to achieve long-life sulfide-based all-solid-state lithium batteries. *J. Mater. Chem. A* **2022**, *10*, 21336–21348. [CrossRef]
111. Wenzel, S.; Leichtweiss, T.; Kruger, D.; Sann, J.; Janek, J. Interphase formation on lithium solid electrolytes-An in situ approach to study interfacial reactions by photoelectron spectroscopy. *Solid State Ion.* **2015**, *278*, 98–105. [CrossRef]
112. Tseng, K.-T.; Lee, K.; Sakamoto, J. Enabling "Sodium-Metal-Free" Manufacturing of Solid-State Batteries. *ACS Energy Lett.* **2024**, *9*, 4544–4549. [CrossRef]
113. Ohta, N.; Takada, K.; Zhang, L.; Ma, R.; Osada, M.; Sasaki, T. Enhancement of the High-Rate Capability of Solid-State Lithium Batteries by Nanoscale Interfacial Modification. *Adv. Mater.* **2006**, *18*, 2226–2229. [CrossRef]
114. Chen, M.; Zhang, J.; Ji, X.; Fu, J.; Feng, G. Progress on predicting the electrochemical stability window of electrolytes. *Curr. Opin. Electrochem.* **2022**, *34*, 101030. [CrossRef]
115. Ye, Q.; Liang, H.; Wang, S.; Cui, C.; Zeng, C.; Zhai, T.; Li, H. Fabricating a PVDF skin for PEO-based SPE to stabilize the interface both at cathode and anode for Li-ion batteries. *J. Energy Chem.* **2022**, *70*, 356–362. [CrossRef]
116. Lin, Y.; Liu, Z.; Leung, K.; Chen, L.; Lu, P.; Qi, Y. Connecting the irreversible capacity loss in Li-ion batteries with the electronic insulating properties of solid electrolyte interphase (SEI) components. *J. Power Sources* **2016**, *309*, 221–230. [CrossRef]
117. Fan, E.; Li, L.; Wang, Z.; Lin, J.; Huang, Y.; Yao, Y.; Chen, R.; Wu, F. Sustainable Recycling Technology for Li-Ion Batteries and Beyond: Challenges and Future Prospects. *Chem. Rev.* **2020**, *120*, 7020–7063. [CrossRef] [PubMed]
118. Nomura, Y.; Yamamoto, K. Advanced Characterization Techniques for Sulfide-Based Solid-State Lithium Batteries. *Adv. Energy Mater.* **2023**, *13*, 2203883. [CrossRef]
119. Qi, X.; Jin, X.; Xu, H.; Pan, Y.; Yang, F.; Zhu, Z.; Ji, J.; Jiang, R.; Du, H.; Ji, Y.; et al. Air-Stable Li_2S Cathodes Enabled by an In Situ-Formed Li^+ Conductor for Graphite-Li_2S Pouch Cells. *Adv. Mater.* **2024**, *36*, 2310756. [CrossRef]
120. Roh, J.; Kim, H.; Lee, H.; Bu, H.; Manjón-Sanz, A.; Kim, H.; Hong, S.-T. Unraveling Polymorphic Crystal Structures of Li_4SiS_4 for All-Solid-State Batteries: Enhanced Ionic Conductivity via Aliovalent Sb Substitution. *Chem. Mater.* **2024**, *36*, 6973–6984. [CrossRef]
121. Hikima, K.; Kusaba, I.; Gamo, H.; Phuc, N.H.H.; Muto, H.; Matsuda, A. High Ionic Conductivity with Improved Lithium Stability of CaS^- and CaI^{2-} Doped $Li_7P_3S_{11}$ Solid Electrolytes Synthesized by Liquid-Phase Synthesis. *ACS Omega* **2022**, *7*, 16561–16567. [CrossRef]
122. Lu, P.; Xia, Y.; Sun, G.; Wu, D.; Wu, S.; Yan, W.; Zhu, X.; Lu, J.; Niu, Q.; Shi, S. Realizing long-cycling all-solid-state Li-In||TiS_2 batteries using $Li_{6+x}M_xAs_{1-x}S_5I$ (M=Si, Sn) sulfide solid electrolytes. *Nat. Commun.* **2023**, *14*, 4077. [CrossRef] [PubMed]
123. Wang, A.; Wang, L.; Wu, Y.; He, Y.; Ren, D.; Song, Y.; Zhang, B.; Xu, H.; He, X. Uncovering the Effect of Solid Electrolyte Interphase on Ion Desolvation for Rational Interface Design in Li-Ion Batteries. *Adv. Energy Mater.* **2023**, *13*, 2300626. [CrossRef]
124. Murayama, M.; Kanno, R.; Irie, M.; Ito, S.; Hata, T.; Sonoyama, N.; Kawamoto, Y. Synthesis of New Lithium Ionic Conductor Thio-LISICON—Lithium Silicon Sulfides System. *J. Solid State Chem.* **2002**, *168*, 140–148. [CrossRef]
125. Ong, S.P.; Mo, Y.; Richards, W.D.; Miara, L.; Lee, H.S.; Ceder, G. Phase Stability, Electrochemical Stability and Ionic Conductivity of the $Li_{10\pm1}MP_2X_{12}$ (M = Ge, Si, Sn, Al or P, and X = O, S or Se) Family of Superionic Conductors. *Energy Environ. Sci.* **2013**, *6*, 148–156. [CrossRef]
126. Wu, Y.; Li, C.; Zheng, X.; Zhao, W.; Wang, H.; Gu, J.; Cheng, Y.; Lin, Y.; Su, Y.; Ren, F.; et al. High Energy Sulfide-Based All-Solid-State Lithium Batteries Enabled by Single-Crystal Li-Rich Cathodes. *ACS Energy Lett.* **2024**, *9*, 5156–5165. [CrossRef]
127. Hanghofer, I.; Brinek, M.; Eisbacher, S.L.; Bitschnau, B.; Volck, M.; Hennige, V.; Hanzu, I.; Rettenwander, D.; Wilkening, H.M.R. Substitutional disorder: Structure and ion dynamics of the argyrodites Li_6PS_5Cl, Li_6PS_5Br and Li_6PS_5I. *Phys. Chem. Chem. Phys.* **2019**, *21*, 8489–8507. [CrossRef]
128. Pecher, O.; Tong, S.; Goebel, T.; Nickel, V.; Weichert, K.; Reiner, C.; Deiseroth, H.-J.; Maier, J.; Haarmann, F.; Zahn, D. Atomistic Characterisation of Li^+ Mobility and Conductivity in $Li_{7-x}PS_{6-x}I_x$ Argyrodites from Molecular Dynamics Simulations, Solid-State NMR, and Impedance Spectroscopy. *Chem. Eur. J.* **2010**, *16*, 8347–8354. [CrossRef]
129. Zhao, Y.; Ye, H.; Zhang, H.; Zhao, D.; Huang, L.; Lee, J.Y. The beneficial effects of black phosphorous modification of the anode current collector in Li-metal free Li_2S-based batteries. *Mater. Today Energy* **2022**, *30*, 101179. [CrossRef]

130. Ma, Z.; Xue, H.; Guo, S. Recent achievements on sulfide-type solid electrolytes: Crystal structures and electrochemical performance. *J. Mater. Sci.* **2018**, *53*, 3927–3938. [CrossRef]
131. Karabelli, D.; Birke, K.P.; Weeber, M. A Performance and Cost Overview of Selected Solid-State Electrolytes: Race between Polymer Electrolytes and Inorganic Sulfide Electrolytes. *J. Batter.* **2021**, *7*, 18. [CrossRef]
132. Zhang, Z.; Wu, L.; Zhou, D.; Weng, W.; Yao, X. Flexible Sulfide Electrolyte Thin Membrane with Ultrahigh Ionic Conductivity for All-Solid-State Lithium Batteries. *Nano Lett.* **2021**, *21*, 5233–5239. [CrossRef] [PubMed]
133. Shu, Y.; He, J.; Xu, D.; Hu, J.; Luo, Q.; Ouyang, Y.; Wan, C. Mechanical and thermal behavior of PBAT matrix composites filled with lignin. *J. Polym. Res.* **2025**, *32*, 56. [CrossRef]
134. Qian, X.; Lyu, Y.; Zhou, S.; Qiu, Y.; Sun, Y.; Yuan, Y.; Shao, M. Enhancing Long Stability of Solid-State Batteries Through High-Energy Ball Milling-Induced Decomposition of Sulfide-Based Electrolyte to Sulfur. *Adv. Mater.* **2024**, *36*, 2412319. [CrossRef] [PubMed]
135. Lyu, N.; Sun, Z.; Hu, Y.; Li, B.; Jing, S.; Zhang, Z.; Jiang, L.; Jia, M.; Liu, F. Preparation and properties of sulfide solid state electrolyte Li_6PS_5Cl by ball milling-solid phase sintering. *J. Mater. Eng.* **2022**, *50*, 103–110.
136. Serbessa, G.G.; Nikodimos, Y.; Taklu, B.W.; Merso, S.K.; Muche, Z.B.; Dandena, B.D.; Vallal, S.A.; Yeh, T.-I.; Valencia, F.; Hung, Y.-F.; et al. Stabilizing the interface between Li_6PS_5Cl argyrodite sulfide solid electrolyte and Li via in situ formed LiF-Li_3Bi lithiophobic-lithiophilic bifunctional layer. *J. Energy Storage Mater.* **2025**, *73*, 104103. [CrossRef]
137. Salam, S.A.; George, C.S.; Al Abdulsalam, N.K.; Abdel-Moneim, A.M.; Essawy, A.E. Ginkgo biloba attenuates complete Freund's adjuvant-induced inflammatory pain by suppressing the NF-κB-CXCL1/CXCR2 signaling cascade in the rat spinal cord. *J. Redox Rep.* **2025**, *30*, 2447778. [CrossRef]
138. Liu, S.; Tian, G.; Chen, J.; Zhang, X.; Wu, A.; Li, M.; Sun, Y.; Liu, B.; Xing, Y.; Shang, H. Traditional Chinese Medicine for Bradyarrhythmia: Evidence and Potential Mechanisms. *Front Pharmacol.* **2018**, *9*, 324. [CrossRef]
139. Shao, Z.; Zhou, W.; Zhu, Z. Advanced synthesis of materials for intermediate-temperature solid oxide fuel cells. *J. Prog. Mater. Sci.* **2012**, *57*, 804–874. [CrossRef]
140. Miller, J.E.; Allendorf, M.D.; Diver, R.B.; Evans, L.R.; Siegel, N.P.; Stuecker, J.N. Metal oxide composites and structures for ultra-high temperature solar thermochemical cycles. *J. Mater. Sci.* **2008**, *43*, 4714–4728. [CrossRef]
141. Wang, D.; Li, Y. Bimetallic Nanocrystals: Liquid-Phase Synthesis and Catalytic Applications. *J. Adv. Mater.* **2011**, *23*, 1044–1060. [CrossRef]
142. Bayer, E.; Mutter, M. Liquid phase synthesis of peptides. *J. Nat.* **1972**, *237*, 512–513. [CrossRef]
143. Miao, W.; Chan, T. Ionic-liquid-supported synthesis: A novel liquid-phase strategy for organic synthesis. *Acc. Chem. Res.* **2006**, *39*, 897–908. [CrossRef]
144. Wang, M.; Chen, M.; Xu, G.; Wu, S. Photoinduced Reversible Solid-to-liquid Transitions of Azopolymers. *Chemistry* **2020**, *83*, 600–609.
145. Calpa, M.; Rosero-Navarro, N.C.; Miura, A.; Tadanaga, K. Instantaneous preparation of high lithium-ion conducting sulfide solid electrolyte Li7P3S11 by a liquid phase process. *J. RSC Adv.* **2017**, *7*, 46499–46504. [CrossRef]
146. Wu, J.; Liu, S.; Han, F.; Yao, X.; Wang, C. Lithium/Sulfide All-Solid-State Batteries using Sulfide Electrolytes. *Adv. Mater.* **2021**, *33*, 2000751. [CrossRef]
147. Gao, C.; Zhang, J.; He, C.; Fu, Y.; Zhou, T.; Li, X.; Kang, S.; Tan, L.; Jiao, Q.; Dai, S.; et al. Unveiling the Growth Mechanism of the Interphase between Lithium Metal and Li_2S-P_2S_5-B_2S_3 Solid-State Electrolytes. *Adv. Energy Mater.* **2023**, *13*, 2204386. [CrossRef]
148. Zhang, Z.; Liu, Z.; Chen, X.; Wei, Y.; Yu, H.; Zhang, J.; Zheng, C. Plasma-Liquid-Induced Synthesis of Scandium-Metalloporphyrin Frameworks for Boosted Sensing and Photosensitization. *Adv. Mater.* **2025**, *37*, 2412071. [CrossRef]
149. Oh, D.Y.; Nam, Y.J.; Park, K.H.; Jung, S.H.; Kim, K.T.; Ha, A.R.; Jung, Y.S. Slurry-Fabricable Li^+-Conductive Polymeric Binders for Practical All-Solid-State Lithium-Ion Batteries Enabled by Solvate Ionic Liquids. *Adv. Energy Mater.* **2019**, *9*, 1802927. [CrossRef]
150. Lee, K.L.; Lee, J.U.; Choi, S.H.; Char, K.; Choi, J.W. Thiol-Ene Click Reaction for Fine Polarity Tuning of Polymeric Binders in Solution-Processed All-Solid-State Batteries. *ACS Energy Lett.* **2019**, *4*, 94–101. [CrossRef]
151. Cho, W.; Park, J.; Kim, K.; Yu, J.-S.; Jeong, G. Sulfide-Compatible Conductive and Adhesive Glue-Like Interphase Engineering for Sheet-Type All-Solid-State Battery. *Small* **2021**, *17*, 1902138. [CrossRef]
152. Shen, Y.Q.; Zeng, F.L.; Zhou, X.Y.; Wang, A.; Wang, W.; Yuan, N.; Ding, J. A novel permselective organo-polysulfides/PVDF gel polymer electrolyte enables stable lithium anode for lithium-sulfur batteries. *J. Energy Chem.* **2020**, *48*, 267–276. [CrossRef]
153. Zhang, J.; Zhu, C.; Xu, J.; Wu, J.; Yin, X.; Chen, S.; Zhu, Z.; Wang, L.; Li, Z. Enhanced mechanical behavior and electrochemical performance of composite separator by constructing crosslinked polymer electrolyte networks on polyphenylene sulfide nonwoven surface. *J. Membr. Sci.* **2020**, *597*, 117622. [CrossRef]
154. Li, M.; Frerichs, J.E.; Kolek, M.; Sun, W.; Zhou, D.; Huang, C.J.; Hwang, B.J.; Hansen, M.R.; Bieker, P. Solid-State Lithium-Sulfur Battery Enabled by Thio-LiSICON/Polymer Composite Electrolyte and Sulfurized Polyacrylonitrile Cathode. *Adv. Funct. Mater.* **2020**, *30*, 1910123. [CrossRef]

155. Tan, D.H.S.; Chen, Y.-T.; Yang, H.; Bao, W.; Sreenarayanan, B.; Doux, J.-M.; Li, W.; Lu, B.; Ham, S.-Y.; Sayahpour, B.; et al. Carbon-free high-loading silicon anodes enabled by sulfide solid electrolytes. *Science* **2021**, *373*, 1494–1499. [CrossRef]
156. Yan, W.; Wu, F.; Li, H.; Chen, L. Application of Si-based anodes in sulfide solid-state batteries. *J. Energy Storage Sci. Technol.* **2021**, *10*, 821–835.
157. Li, H.; Lin, Q.; Wang, J.; Hu, L.; Chen, F.; Zhang, Z.; Ma, C. A Cost-Effective Sulfide Solid Electrolyte $Li_7P_3S_{7.5}O_{3.5}$ with Low Density and Excellent Anode Compatibility. *Angew. Chem. Int. Ed.* **2024**, *63*, e202407892. [CrossRef]
158. Shao, B.; Das, R.; Huang, Y.; Deng, R.; Seelman, S.; Han, F. Structural evolution during solution-based synthesis of $Li_7P_3S_{11}$ solid electrolyte by synchrotron X-ray total scattering. *J. Mater. Chem. A* **2023**, *11*, 17035–17044. [CrossRef]
159. Sun, K.; Xiao, X.; Shang, W.; Fu, K.; Li, X.; Zhang, Z.; Gong, L.; Tan, P. Unveiling the Interplay Between Silicon and Graphite in Composite Anodes for Lithium-Ion Batteries. *Small* **2024**, *20*, 2405674. [CrossRef]
160. Ma, R.; Chang, L.; Ye, S.; Xie, H.; Xiao, Q.; Zhang, L.; Si, J.; Yu, P. Magnetic properties of soft magnetic composites fabricated from amorphous $Fe_{73}Si_{11}B_{11}C_3Cr_2$ powder by hot pressing under a low pressure. *Powder Technol.* **2023**, *426*, 118639. [CrossRef]
161. Nikodimos, Y.; Huang, C.-J.; Taklu, B.W.; Su, W.-N.; Hwang, B.J. Chemical stability of sulfide solid-state electrolytes: Stability toward humid air and compatibility with solvents and binders. *Energy Environ. Sci.* **2022**, *15*, 991–1033. [CrossRef]
162. Hirano, M.; Inagaki, M.; Mizutani, Y.; Nomura, K.; Kawai, M.; Nakamura, Y. Mechanical and electrical properties of Sc_2O_3-doped zirconia ceramics improved by postsintering with HIP. *Solid State Ion.* **2000**, *133*, 1–9. [CrossRef]
163. Yang, W.; Li, Z.; Lai, C.; Zhao, R.; Li, Y.; Zhou, Y.; Huang, Y.; Zhu, L.; Feng, W.; Wang, W.; et al. Comparative study on self-discharge rate of new CF x lithium primary batteries and recommendations for their use. *Energy Storage Sci. Technol.* **2024**, *13*, 3742–3753.
164. Cao, D.; Zhao, Y.; Sun, X.; Natan, A.; Wang, Y.; Xiang, P.; Wang, W.; Zhu, H. Processing Strategies to Improve Cell-Level Energy Density of Metal Sulfide Electrolyte-Based All-Solid-State Li Metal Batteries and Beyond. *ACS Energy Lett.* **2020**, *5*, 3468–3489. [CrossRef]
165. Song, Y.B.; Baeck, K.H.; Kwak, H.; Lim, H.; Jung, Y.S. Dimensional Strategies for Bridging the Research Gap between Lab-Scale and Potentially Practical All-Solid-State Batteries: The Role of Sulfide Solid Electrolyte Films. *Adv. Energy Mater.* **2023**, *13*, 2301142. [CrossRef]
166. Pei, F.; Huang, Y.; Wu, L.; Zhou, S.; Kang, Q.; Lin, W.; Liao, Y.; Zhang, Y.; Huang, K.; Shen, Y.; et al. Multisite Crosslinked Poly(ether-urethane)-Based Polymer Electrolytes for High-Voltage Solid-State Lithium Metal Batteries. *Adv. Mater.* **2024**, *36*, 2409269. [CrossRef]
167. Guo, R.; Zhang, K.; Zhao, W.; Hu, Z.; Li, S.; Zhong, Y.; Yang, R.; Wang, X.; Wang, J.; Wu, C.; et al. Interfacial Challenges and Strategies toward Practical Sulfide-Based Solid-State Lithium Batteries. *Energy Mater Adv.* **2023**, *4*, 0022. [CrossRef]
168. Zhao, Z.; Chen, Z.; Zhai, G.; Zhang, X.; Zhuang, X. Preparation of Sc/O-doped sulfide electrolyte for all-solid-state batteries. *Energy Storage Sci. Technol.* **2023**, *12*, 2412–2423.
169. Wang, L.; Xie, R.; Chen, B.; Yu, X.; Ma, J.; Li, C.; Hu, Z.; Sun, X.; Xu, C.; Dong, S.; et al. In-situ visualization of the space-charge-layer effect on interfacial lithium-ion transport in all-solid-state batteries. *Nat. Commun.* **2020**, *11*, 5889. [CrossRef]
170. Li, J.; Li, Y.; Zhang, S.; Liu, T.; Li, D.; Ci, L. Long cycle life all-solid-state batteries enabled by solvent-free approach for sulfide solid electrolyte and cathode films. *Chem. Eng. J.* **2023**, *455*, 140605. [CrossRef]
171. Gogotsi, Y.; Penner, R.M. Energy Storage in Nanomaterials-Capacitive, Pseudocapacitive, or Battery-like? *ACS Nano* **2018**, *12*, 2081–2083. [CrossRef]
172. Gao, B.; Jalem, R.; Ma, Y.; Tateyama, Y. Li^+ Transport Mechanism at the Heterogeneous Cathode/Solid Electrolyte Interface in an All-Solid-State Battery via the First-Principles Structure Prediction Scheme. *Chem. Mater.* **2020**, *32*, 85–96. [CrossRef]
173. Zhang, J.; Zheng, C.; Li, L.; Xia, Y.; Huang, H.; Gan, Y.; Liang, C.; He, X.; Tao, X.; Zhang, W. Unraveling the Intra and Intercycle Interfacial Evolution of Li_6PS_5Cl-Based All-Solid-State Lithium Batteries. *Adv. Energy Mater.* **2020**, *10*, 1903311. [CrossRef]
174. Yang, X.; Yin, Q.; Wang, C.; Doyle-Davis, K.; Sun, X.; Li, X. Towards practically accessible high-voltage solid-state lithium batteries: From fundamental understanding to engineering design. Prog. *Mater. Sci.* **2023**, *140*, 101193. [CrossRef]
175. Haruyama, J.; Sodeyama, K.; Han, L.; Takada, K.; Tateyama, Y. Space-Charge Layer Effect at Interface between Oxide Cathode and Sulfide Electrolyte in All-Solid-State Lithium-Ion Battery. *Chem. Mater.* **2014**, *26*, 4248–4255. [CrossRef]
176. Gao, B.; Jalem, R.; Tateyama, Y. First-Principles Study of Microscopic Electrochemistry at the $LiCoO_2$ Cathode/$LiNbO_3$ Coating/β-Li_3PS_4 Solid Electrolyte Interfaces in an All-Solid-State Battery. *ACS Appl. Mater. Interfaces* **2021**, *13*, 11765–11773. [CrossRef] [PubMed]
177. Takada, K.; Ohno, T.; Ohta, N.; Ohnishi, T.; Tanaka, Y. Positive and Negative Aspects of Interfaces in Solid-State Batteries. *ACS Energy Lett.* **2018**, *3*, 98–103. [CrossRef]
178. Li, X.; Jin, L.; Song, D.; Zhang, H.; Shi, X.; Wang, Z.; Zhang, L.; Zhu, L. $LiNbO_3$-coated $LiNi_{0.8}Co_{0.1}Mn_{0.1}O_2$ cathode with high discharge capacity and rate performance for all-solid-state lithium battery. *J. Energy Chem.* **2020**, *40*, 39–45. [CrossRef]
179. Zhu, Y.; He, X.; Mo, Y. Origin of Outstanding Stability in the Lithium Solid Electrolyte Materials: Insights from Thermodynamic Analyses Based on First-Principles Calculations. *ACS Appl. Mater. Interfaces* **2015**, *7*, 23685–23693. [CrossRef]

180. Wang, C.; Hwang, S.; Jiang, M.; Liang, J.; Sun, Y.; Adair, K.; Zheng, M.; Mukherjee, S.; Li, X.; Li, R.; et al. Deciphering Interfacial Chemical and Electrochemical Reactions of Sulfide-Based All-Solid-State Batteries. *Adv. Energy Mater.* **2021**, *11*, 2100210. [CrossRef]
181. Zhang, X.; Li, X.; Weng, S.; Wu, S.; Liu, Q.; Cao, M.; Li, Y.; Wang, Z.; Zhu, L.; Xiao, R.; et al. Spontaneous gas-solid reaction on sulfide electrolytes for high-performance all-solid-state batteries. *Energy Environ. Sci.* **2023**, *16*, 1091–1099. [CrossRef]
182. Sakuda, A.; Hayashi, A.; Tatsumisago, M. Interfacial Observation between $LiCoO_2$ Electrode and Li_2S-P_2S_5 Solid Electrolytes of All-Solid-State Lithium Secondary Batteries Using Transmission Electron Microscopy. *Chem. Mater.* **2010**, *22*, 949–956. [CrossRef]
183. Famprikis, T.; Canepa, P.; Dawson, J.A.; Islam, M.S.; Masquelier, C. Fundamentals of inorganic solid-state electrolytes for batteries. *Nat. Mater.* **2019**, *18*, 1278–1291. [CrossRef]
184. Minnmann, P.; Strauss, F.; Bielefeld, A.; Ruess, R.; Adelhelm, P.; Burkhardt, S.; Dreyer, S.L.; Trevisanello, E.; Ehrenberg, H.; Brezesinski, T.; et al. Designing Cathodes and Cathode Active Materials for Solid-State Batteries. *Adv. Energy Mater.* **2022**, *12*, 2201425. [CrossRef]
185. Zhu, Y.; He, X.; Mo, Y. First principles study on electrochemical and chemical stability of solid electrolyte-electrode interfaces in all-solid-state Li-ion batteries. *J. Mater. Chem. A* **2016**, *4*, 3253–3266. [CrossRef]
186. Dietrich, C.; Weber, D.A.; Culver, S.; Senyshyn, A.; Sedlmaier, S.J.; Indris, S.; Janek, J.; Zeier, W.G. Synthesis, Structural Characterization, and Lithium Ion Conductivity of the Lithium Thiophosphate $Li_2P_2S_6$. *Inorg. Chem.* **2017**, *56*, 6681–6687. [CrossRef]
187. Lu, T.; Meng, S.; Liu, M. Electrochemically and chemically stable electrolyte-electrode interfaces for lithium iron phosphate all-solid-state batteries with sulfide electrolytes. *J. Mater. Chem. A* **2024**, *12*, 3954–3966. [CrossRef]
188. Zhang, H.; Zhang, J. An overview of modification strategies to improve $LiNi_{0.8}Co_{0.1}Mn_{0.1}O_2$ (NCM811) cathode performance for automotive lithium-ion batteries. *ETransportation* **2021**, *7*, 100105. [CrossRef]
189. Porz, L.; Swamy, T.; Sheldon, B.W.; Rettenwander, D.; Frömling, T.; Thaman, H.L.; Berendts, S.; Uecker, R.; Carter, W.C.; Chiang, Y.M. Mechanism of Lithium Metal Penetration through Inorganic Solid Electrolytes. *Adv. Energy Mater.* **2017**, *7*, 1701003. [CrossRef]
190. Swamy, T.; Park, R.; Sheldon, B.W.; Rettenwander, D.; Porz, L.; Berendts, S.; Uecker, R.; Carter, W.C.; Chiang, Y.M. Lithium Metal Penetration Induced by Electrodeposition through Solid Electrolytes: Example in Single-Crystal $Li_6La_3ZrTaO_{12}$ Garnet. *J. Electrochem. Soc.* **2018**, *165*, A3648. [CrossRef]
191. Lu, Y.; Zhao, C.Z.; Hu, J.K.; Sun, S.; Yuan, H.; Fu, Z.H.; Chen, X.; Huang, J.Q.; Ouyang, M.; Zhang, Q. The void formation behaviors in working solid-state Li metal batteries. *Sci. Adv.* **2022**, *8*, add0510. [CrossRef] [PubMed]
192. Zhu, Y.; Li, W.; Zhang, L.; Fang, W.; Ruan, Q.; Li, J.; Zhang, F.; Zhang, H.; Quan, T.; Zhang, S. Electrode/electrolyte interphases in high-temperature batteries: A review. *Energy Environ. Sci.* **2023**, *16*, 2825–2855. [CrossRef]
193. Cheng, X.-B.; Zhao, C.-Z.; Yao, Y.-X.; Liu, H.; Zhang, Q. Recent Advances in Energy Chemistry between Solid-State Electrolyte and Safe Lithium-Metal Anodes. *Chem* **2019**, *5*, 74–96. [CrossRef]
194. Larink, D.; Eckert, H.; Martin, S.W. Structure and Ionic Conductivity in the Mixed-Network Former Chalcogenide Glass System $[Na_2S]_{2/3}[(B_2S_3)_x(P_2S_5)_{1-x}]_{1/3}$. *J. Phys. Chem. C* **2012**, *116*, 22698–22710. [CrossRef]
195. Wang, C.; Liang, J.; Zhao, Y.; Zheng, M.; Li, X.; Sun, X. All-solid-state lithium batteries enabled by sulfide electrolytes: From fundamental research to practical engineering design. *Energy Environ. Sci.* **2021**, *14*, 2577–2619. [CrossRef]
196. Kaup, K.; Bazak, J.D.; Vajargah, S.H.; Wu, X.; Kulisch, J.; Goward, G.R.; Nazar, L.F. A Lithium Oxythioborosilicate Solid Electrolyte Glass with Superionic Conductivity. *Adv. Energy Mater.* **2020**, *10*, 1902783. [CrossRef]
197. See, K.A.; Wu, H.-L.; Lau, K.C.; Shin, M.; Cheng, L.; Balasubramanian, M.; Gallagher, K.G.; Curtiss, L.A.; Gewirth, A.A. Effect of Hydrofluoroether Cosolvent Addition on Li Solvation in Acetonitrile-Based Solvate Electrolytes and Its Influence on S Reduction in a Li–S Battery. *ACS Appl. Mater. Interfaces* **2016**, *8*, 34360–34371. [CrossRef]
198. Feng, X.; Chien, P.-H.; Patel, S.; Zheng, J.; Immediato-Scuotto, M.; Xin, Y.; Hung, I.; Gan, Z.; Hu, Y.-Y. Synthesis and Characterizations of Highly Conductive and Stable Electrolyte $Li_{10}P_3S_{12}I$. *Energy Storage Mater.* **2019**, *22*, 397–401. [CrossRef]
199. Liu, M.; Hong, J.J.; Sebti, E.; Zhou, K.; Wang, S.; Feng, S.; Pennebaker, T.; Hui, Z.; Miao, Q.; Lu, E.; et al. Surface molecular engineering to enable processing of sulfide solid electrolytes in humid ambient air. *Nat. Commun.* **2025**, *16*, 213. [CrossRef]
200. Muramatsu, H.; Hayashi, A.; Ohtomo, T.; Hama, S.; Tatsumisago, M. Structural change of Li_2S-P_2S_5 sulfide solid electrolytes in the atmosphere. *Solid State Ion.* **2011**, *182*, 116–119. [CrossRef]
201. Li, Y.; Wu, H.; Wu, D.; Wei, H.; Guo, Y.; Chen, H.; Li, Z.; Wang, L.; Xiong, C.; Meng, Q.; et al. High-Density Oxygen Doping of Conductive Metal Sulfides for Better Polysulfide Trapping and Li2S-S8 Redox Kinetics in High Areal Capacity Lithium-Sulfur Batteries. *Adv. Sci.* **2022**, *9*, 2200840. [CrossRef] [PubMed]
202. Luo, M.; Wang, C.; Duan, Y.; Zhao, X.; Wang, J.; Sun, X. Surface Coating Enabling Sulfide Solid Electrolytes with Excellent Air Stability and Lithium Compatibility. *Energy Environ. Mater.* **2024**, *7*, e12753. [CrossRef]
203. Yu, N.; Huang, C.; Liu, H.; Liang, Y.; Fan, L.-Z. A High Air-Stability and Li-Metal-Compatible $Li_{3+2x}P_{1-x}Bi_xS_{4-1.5x}O_{1.5x}$ Sulfide Electrolyte for All-Solid-State Li–Metal Batteries. *Adv. Funct. Mater.* **2022**, *32*, 2205998.

204. Ohtomo, T.; Hayashi, A.; Tatsumisago, M.; Kawamoto, K. All-solid-state batteries with Li_2O-Li_2S-P_2S_5 glass electrolytes synthesized by two-step mechanical milling. *J. Solid State Electrochem.* **2013**, *17*, 2551–2557. [CrossRef]
205. Zhou, L.; Zhang, Q.; Nazar, L.F. Li-rich and halide-deficient argyrodite fast ion conductors. *Chem. Mater.* **2022**, *34*, 9634–9643. [CrossRef]
206. Kraft, M.A.; Ohno, S.; Zinkevich, T.; Koerver, R.; Culver, S.P.; Fuchs, T.; Senyshyn, A.; Indris, S.; Morgan, B.J.; Zeier, W.G. Inducing High Ionic Conductivity in the Lithium Superionic Argyrodites $Li_{6+x}P_{1-x}Ge_xS_5I$ for All-Solid-State Batteries. *J. Am. Chem. Soc.* **2018**, *140*, 16330–16339. [CrossRef]
207. Xu, R.; Xia, X.; Wang, X.; Xia, Y.; Tu, J. Tailored Li_2S-P_2S_5 glass-ceramic electrolyte by MoS_2 doping, possessing high ionic conductivity for all-solid-state lithium-sulfur batteries. *J. Mater. Chem. A* **2017**, *5*, 2829–2834. [CrossRef]
208. Xie, D.; Chen, S.; Zhang, Z.; Ren, J.; Yao, L.; Wu, L.; Yao, X.; Xu, X. High ion conductive Sb_2O_5-doped β-Li_3PS_4 with excellent stability against Li for all-solid-state lithium batteries. *J. Power Sources* **2018**, *389*, 140–147. [CrossRef]
209. Bai, W.; Gao, J.; Li, K.; Wang, G.; Zhou, T.; Li, P.; Qin, S.; Zhang, G.; Guo, Z.; Xiao, C.; et al. Natural Soft/Rigid Superlattices as Anodes for High-Performance Lithium-Ion Batteries. *Angew. Chem.* **2020**, *59*, 17494–17498. [CrossRef]
210. Gautam, A.; Sadowski, M.; Ghidiu, M.; Minafra, N.; Senyshyn, A.; Albe, K.; Zeier, W.G. Engineering the Site-Disorder and Lithium Distribution in the Lithium Superionic Argyrodite Li_6PS_5Br. *Adv. Energy Mater.* **2020**, *11*, 2003369. [CrossRef]
211. Paul, P.P.; Chen, B.R.; Langevin, S.A.; Dufek, E.J.; Weker, J.N.; Ko, J.S. Interfaces in all solid-state Li-metal batteries: A review on instabilities, stabilization strategies, and scalability. *Energy Storage Mater.* **2022**, *45*, 969–1001. [CrossRef]
212. Lee, K.-J.; Byeon, Y.-W.; Lee, H.-J.; Lee, Y.; Park, S.; Kim, H.-R.; Kim, H.-K.K.; Oh, S.J.; Ahn, J.-P. Revealing crack-healing mechanism of NCM composite cathode for sustainable cyclability of sulfide-based solid-state batteries. *Energy Storage Mater.* **2023**, *57*, 326–333. [CrossRef]
213. Gu, J.; Zhong, H.; Chen, Z.; Shi, J.; Gong, Z.; Yang, Y. Advances in sulfide-based all-solid-state lithium-sulfur battery: Materials, composite electrodes and electrochemo-mechanical effects. *Chem. Eng. J.* **2023**, *454*, 139923. [CrossRef]
214. Jiang, Z.; Peng, H.; Liu, Y.; Li, Z.; Zhong, Y.; Wang, X.; Xia, X.; Gu, C.; Tu, J. A Versatile $Li_{6.5}In_{0.25}P_{0.75}S_5I$ Sulfide Electrolyte Triggered by Ultimate-Energy Mechanical Alloying for All-Solid-State Lithium Metal Batteries. *Adv. Energy Mater.* **2021**, *11*, 2101521. [CrossRef]
215. Wang, J.; Yang, K.; Sun, S.; Ma, Q.; Yi, G.; Chen, X.; Wang, Z.; Yan, W.; Liu, X.; Cai, Q.; et al. Advances in thermal-related analysis techniques for solid-state lithium batteries. *J. InfoMat.* **2023**, *5*, e12401. [CrossRef]
216. Gao, J.; Kedir, N.; Kirk, C.D.; Hernandez, J.; Wang, J.; Paulson, S.; Zhai, X.; Horn, T.; Kim, G.; Gao, J.; et al. Real-time damage characterization for GFRCs using high-speed synchrotron X-ray phase contrast imaging. *J. Compos. Part B Eng.* **2021**, *207*, 108565. [CrossRef]
217. Wu, D.; Chen, L.; Li, H.; Wu, F. Solid-state lithium batteries: From fundamental research to industrial progress. *Prog. Mater. Sci.* **2023**, *139*, 101182. [CrossRef]
218. Wang, C.C.; Liu, Y.; Jeong, W.J.; Chen, T.; Lu, M.; Nelson, D.L.; Alsaç, E.P.; Yoon, S.G.; Cavallaro, K.A.; Das, S.; et al. The influence of pressure on lithium dealloying in solid-state and liquid electrolyte batteries. *Nat. Mater.* **2025**, 1–10. [CrossRef]
219. Lu, T.; Chen, X.; Wang, H.; Zhang, L.; Zhou, Y. Comparison of low-velocity impact damage in thermoplastic and thermoset composites by non-destructive three-dimensional X-ray microscope. *J. Polym. Test.* **2020**, *91*, 106730. [CrossRef]
220. Guo, Y.; Wu, S.; He, Y.-B.; Kang, F.; Chen, L.; Li, H.; Yang, Q.-H. Solid-state lithium batteries: Safety and prospects. *EScience* **2022**, *2*, 138–163. [CrossRef]
221. Sun, Y.-Y.; Zhang, Q.; Yan, L.; Wang, T.-B.; Hou, P.-Y. A review of interfaces within solid-state electrolytes: Fundamentals, issues and advancements. *J. Chem. Eng. J.* **2022**, *437*, 135179. [CrossRef]
222. McCue, I.; Karma, A.; Erlebacher, J. Pattern formation during electrochemical and liquid metal dealloying. *MRS Bull.* **2018**, *43*, 27–34. [CrossRef]
223. McCue, I.; Benn, E.; Gaskey, B.; Erlebacher, J. Dealloying and dealloyed materials. *Ann. Rev. Mater. Res.* **2016**, *46*, 263–286. [CrossRef]
224. Wang, C.; Zhu, G.; Liu, P.; Chen, Q. Monolithic nanoporous Zn anode for rechargeable alkaline batteries. *ACS Nano* **2020**, *14*, 2404–2411. [CrossRef]
225. McDowell, M.T.; Lee, S.W.; Nix, W.D.; Cui, Y. 25th anniversary article: Understanding the lithiation of silicon and other alloying anodes for lithium-ion batteries. *Adv. Mater.* **2013**, *25*, 4966–4985. [CrossRef]
226. Shi, J.; Jiang, K.; Fan, Y.; Zhao, L.; Cheng, Z.X.; Yu, P.; Peng, J.; Wan, M. Advancing Metallic Lithium Anodes: A Review of Interface Design, Electrolyte Innovation, and Performance Enhancement Strategies. *Molecules* **2024**, *29*, 3624. [CrossRef]
227. Zhou, Q.; Xiong, X.; Peng, J.; Wu, W.; Fan, W.; Yang, H.; Wang, T.; Ma, Y.; Wang, F.; Wu, Y. Tailored Engineering on the Interface Between Lithium Metal Anode and Solid-State Electrolytes. *Energy Environ. Mater.* **2025**, *8*, e12831. [CrossRef]
228. Zhou, X.; Yan, S.; He, X.; Zhou, H.; Ning, J.; Li, H.; Wang, K.; Jiang, K. Low-temperature, high cycling stability, and high Coulombic efficiency liquid metal batteries enabled by lithium halide-potassium halide molten salt electrolytes. *Energy Storage Mater.* **2023**, *61*, 102889. [CrossRef]

229. Zhu, X.; Wang, L.; Bai, Z.; Lu, J.; Wu, T. Sulfide-Based All-Solid-State Lithium-Sulfur Batteries: Challenges and Perspectives. *Nano-Micro Lett.* **2023**, *15*, 75. [CrossRef]
230. Zheng, Y.; Yao, Y.; Ou, J.; Li, M.; Luo, D.; Dou, H.; Li, Z.; Amine, K.; Yu, A.; Chen, Z. A review of composite solid-state electrolytes for lithium batteries: Fundamentals, key materials and advanced structures. *Chem. Soc. Rev.* **2020**, *49*, 8790–8839. [CrossRef]
231. Matios, E.; Wang, H.; Wang, C.; Li, W. Enabling Safe Sodium Metal Batteries by Solid Electrolyte Interphase Engineering: A Review. *Ind. Eng. Chem. Res.* **2019**, *58*, 9758–9780. [CrossRef]
232. Leng, J.; Liang, H.; Wang, H.; Xiao, Z.; Wang, S.; Zhang, Z.; Tang, Z. A facile and low-cost wet-chemistry artificial interface engineering for garnet-based solid-state Li metal batteries. *Nano Energy* **2022**, *101*, 107603. [CrossRef]
233. Li, H.; Zhou, D.; Zhang, M.; Liu, B.; Zhang, C. Multi-field interpretation of internal short circuit and thermal runaway behavior for lithium-ion batteries under mechanical abuse. *Energy* **2023**, *263*, 126027. [CrossRef]
234. Schmidt, C.P.; Sinzig, S.; Gravemeier, V.; Wall, W.A. A three-dimensional finite element formulation coupling electrochemistry and solid mechanics on resolved microstructures of all-solid-state lithium-ion batteries. *Comput. Methods Appl. Mech. Eng.* **2023**, *417*, 116468. [CrossRef]
235. Zou, X.; Ma, C.; Xu, T.; Li, R.; Wang, H.; Chen, F. Evolution mechanism and response strategy of interface mechanics in all solid-state lithium metal batteries. *J. Energy Storage* **2023**, *74*, 109483. [CrossRef]
236. Sun, Q.; Zeng, G.; Xu, X.; Li, J.; Biendicho, J.J.; Wang, S.; Tian, Y.; Ci, L.; Cabot, A. Are Sulfide-Based Solid-State Electrolytes the Best Pair for Si Anodes in Li-Ion Batteries? *Adv. Energy Mater.* **2024**, *14*, 2470176. [CrossRef]
237. Wu, Y.; Zhang, Z.; Zhang, Q.; Zhang, Z.; Li, J.; Liu, M.; Li, H.; Chen, L.; Wu, F. Industrialization challenges for sulfide-based all solid state battery. *eTransportation* **2024**, *22*, 100371. [CrossRef]
238. Yu, P.; Ahmad, N.; Yang, J.; Zeng, C.; Liang, X.; Huang, W.; Ni, M.; Mao, P.; Yang, W. Dual-doping for enhancing chemical stability of functional anionic units in sulfide for high-performance all-solid-state lithium batteries. *J. Energy Chem.* **2023**, *86*, 382–390. [CrossRef]
239. Zeng, D.; Yao, J.; Zhang, L.; Xu, R.; Wang, S.; Yan, X.; Yu, C.; Wang, L. Promoting Favorable Interfacial Properties in Lithium-Based Batteries Using Chlorine-Rich Sulfide Inorganic Solid-State Electrolytes. *Nat. Commun.* **2022**, *13*, 1909. [CrossRef]
240. Zheng, J.; Zhu, X.; Wang, L.; Lu, J.; Wu, T. Insights into interfacial physiochemistry in sulfide solid-state batteries: A review. *Mater. Chem. Front.* **2023**, *7*, 4810–4832. [CrossRef]

Disclaimer/Publisher's Note: The statements, opinions and data contained in all publications are solely those of the individual author(s) and contributor(s) and not of MDPI and/or the editor(s). MDPI and/or the editor(s) disclaim responsibility for any injury to people or property resulting from any ideas, methods, instructions or products referred to in the content.